



TALLINNA TEHNIKAÜLIKOOL
INSENERITEADUSKOND

Mehaanika ja tööstustehnika instituut

LAEVA KÜLJEKORPUSE AVADE MODELLEERIMINE GLOBAALSES LÕPLIKE ELEMENTIDE MUDELIS

MODELING OF SHIP'S SIDE SHELL OPENINGS IN GLOBAL FINITE ELEMENT MODELS

MAGISTRITÖÖ

Üliõpilane: Martin Kaldoja

Üliõpilaskood: 153653MATM

Juhendaja: Hendrik Naar

Tallinn, 2017

AUTORIDEKLARATSIOON

Olen koostanud lõputöö iseseisvalt.

Lõputöö alusel ei ole varem akadeemilist kraadi taotletud. Kõik töö koostamisel kasutatud teiste autorite tööd, olulised seisukohad, kirjandusallikatest ja mujalt pärinevad andmed on viidatud.

“.....” 201.....

Autor:
/ allkiri /

Töö vastab magistritööle esitatud nõuetele

“.....” 201.....

Juhendaja:
/ allkiri /

Kaitsmisele lubatud

“.....”201.....

Kaitsmiskomisjoni esimees
/ nimi ja allkiri /

LÕPUTÖÖ ÜLESANNE

Üliõpilane: Martin Kaldoja, 153653
Õppekava: Tootearendus ja tootmistehnika
Peeriala: Laevaehitus
Juhendaja: Dotsent Hendrik Naar
Konsultandid: Struktuuri analüütik, Eero Avi, Meyer Turku Oy

Lõputöö teema:

Laeva küljekorpuse avade modelleerimine globaalses lõplike elementide mudelis

Modeling of ship's side shell openings in global finite element models

Lõputöö põhieesmärgid:

1. Uurida ja arendada laeva küljekorpuse avade modelleerimistehnikaid
2. Hinnata käsitletud tehnikate rakendatavust reisilaevade küljekorpuse modelleerimisel

Lõputöö etapid ja ajakava:

Ülesande number	Kirjeldus	Tähtaeg
1	Teooriaga tutvumine ning kirjanduse ülevaade; modelleerimistehnikate testimine	27.02.17
2	Lahendavate probleemide püstitus ja valideerimismeetodite välja töötamine	15.03.17
3	Jämeda võrega modelleerimise rakendamine ja analüüs	1.04.17
4	Ekvivalentse ortotroopse tehnika arendus, rakendamine ja tulemuste analüüs	15.05.17
5	Ilmnenud probleemide identifitseerimine ja lahendamine	15.07.17
6	Töö lõpule viimine	22.08.17

Kaitsmistaotlus esitada dekanaati hiljemalt 22.12.2017. Lõputöö esitamise tähtaeg 03.01.2018

Töö keel: Inglise keel

Üliõpilane: Martin Kaldoja "....."201....a
/allkiri/

Juhendaja: Hendrik Naar "....."201....a
/allkiri/

TABLE OF CONETNTS

PREFACE	6
LÜHIKOKKUVÕTE.....	7
ABSTRACT.....	8
TABLE OF FIGURES.....	9
LIST OF TABLES	12
1. INTRODUCTION.....	14
1.1 Background.....	14
1.2 State of the art	16
1.2.1 Domain decomposition method.....	16
1.2.2 Direct modelling with coarse mesh	17
1.2.3 Modelling with equivalent orthotropic elements	18
1.2.4 Second order computational homogenization method	21
1.3 Aim of thesis.....	22
2. METHODS.....	24
2.1 Membrane finite elements for plane stress analysis	24
2.2. Equivalent orthotropic material modeling	28
2.2.1 Equivalent orthotropic element internal forces and strains relation.....	29
2.3 Homogenization	30
2.3.1 Equivalent stress, strain and strain energy	30
2.3.2 Homogenization of orthotropic RVE with central opening	34
2.3.3 Homogenization of RVE with offset openings and stiffeners.....	38
2.4 Limitations in equivalent orthotropic modeling.....	46
2.4.1 Equivalency in forces and moments.....	46
2.4.2 Periodicity of structure and load	48
2.5 Inclusion of stiffeners and window frames in equivalent modelling.....	50
3. DIRECT MODELING OF OPENINGS WITH COARSE MESH	51
3.1 Effect of simplification of structure to shear stiffness	51
3.2 Effect of coarse mesh size to shear stiffness.....	54
4. RESULTS	55

4.1 Equivalent in plane properties	55
4.2 Coarse mesh modeling accuracy	56
4.2.1 The reference model	56
4.2.2 Effect of simplification to shear stiffness	57
4.2.3 Effect of coarse mesh size to shear stiffness.....	58
4.3 Case study 1 - Periodic side shell.....	59
4.3.1 Axial response	60
4.3.2 Shear response	60
4.4 Case study 2 - Box ship with periodic side shell (4-point bending) for evaluation of periodic side shell performance	62
4.4.1 Performance of modeling techniques in periodic grid and boundary of grid	65
4.4.2 Performance of modeling techniques at high strain gradient areas.....	72
5. CONCLUSIONS	75
5. KOKKUVÕTE.....	77
Bibliography	79
APPENDIX 1. SCANTLINGS OF BOX-LIKE SHIP	82

PREFACE

Topic of the present thesis is: Modeling of ship's side shell openings in global finite element model.

The thesis was made at the Department of Applied Mechanics of Aalto University. The research work made in this thesis was funded by Meyer Turku Shipyard.

I would like to thank my advisors and supervisors Jani Romanoff, Eero Avi, Hendrik Naar and Ari Niemelä for their valuable advice, guidance and support during the research process. Special thanks go to Jani Romanoff who lead me to this interesting and challenging research topic.

I am grateful to my family and friends who have provided invaluable support during my studies in Finland.

Turku, 2017

Martin Kaldoja

LÜHIKOKKUVÕTE

Käesolevas magistritöös on uuritud kahte meetodit reisilaevade perioodiliste küljekorpuse avade modelleerimiseks lõplike elementide (LE) mudelis, mida saab kasutada tugevusarvutusteks laeva varajases projekteerimisfaasis. Esimene meetod seisneb küljekorpuse struktuuri homogeniseerimisel ning korpuse modelleerimisel homogeniseeritud ortotroopse materjaliga, rakendades 4- ja 8-sõlmpunktiga elemente. Teine meetod baseerub küljekorpuse avade otseses modelleerimises, kasutades jämedat lõplike elementide võrku ja võttes arvesse geomeetria lihtsustuse ning võrgu suuruse mõju struktuuri jäikusele.

Esitatud meetodid rakendati kahte tüüpi konstruktsiooni jaoks ja tulemuste valideerimiseks kasutati tiheda võrgu LE-analüüsi. Esimeseks uuriti perioodiliste avadega küljekorpust, et hinnata membraanjäikuse korrektsust ühtlase tõmbe- ja lõikepinge seisundites. Teiseks uuriti meetodite täpsust prismaatilise laeva mudelis 4-punkti painde all. Meetodite täpsuse hindamisel on võrreldud prismaatilise mudeli läbipainet, pikisuunalisi normaaljõudusid tekkides ja küljekorpuse vertikaalseid XY-lõikejõude. Lisaks uuriti meetodite täpsust perioodilise struktuuri äärtes ja suure moondegradiendiga piirkondades.

Tulemused näitasid, et lihtne ortotroopne mudel, kus moondegradiendid on väikesed, annab hea täpsusega globaalse läbipainde ja paindepingete jaotuse tekkides nii tsentraalsete kui ka ekstsentriliste avade korral. Ortotroopse mudeli täpsus väheneb juhul kui moondegradiendid on suured nt sisemised pikivaheseinad pole pidevad. Ortotroopse mudeli täpsus lokaalsete sisejõudude mõttes on rahuldav perioodilises struktuuris, kuid langeb oluliselt võre äärtes ja suure moondegradiendiga piirkondades. Ekstsentriliste avade korral avalduvad lisaks eelmainitule ebatäpsused ka mikropolaarse efekti tõttu: ekvivalentsus saavutatakse ainult keskmistatud sisejõudude kuid mitte momentide suhtes. Ortotroopse mudeli täpsus ei sõltu oluliselt ekvivalentse elemendi sõlmpunktide arvust.

Jämeda võrguga mudelile tehti tundlikkusanalüüs, võttes arvesse struktuuri lihtsustuse ja võrgu suuruse mõju. Sobilik kompromiss modelleerimise ajast, arvutuse mahukusest ja täpsusest, leiti võrgu suurusel 4x4 elementi ava kohta. Sellise võrguga mudel osutus 12% jäigemaks ühtlase lõikepinge seisundis. Hoolimata sellest andis jämeda võrguga modelleerimine usaldusväärseid tulemusi prismaatilise laeva mudelis ning täpsus ei sõltunud suuresti moondegradiendist ega ääre-efektist nagu ortotroopse mudeli korral.

Märksõnad: Kruiisilaev, lõplike elementide analüüs, ekvivalentne ortotroopne modelleerimine, jämeda võrguga modelleerimine

ABSTRACT

This thesis presents and investigates two common techniques of modeling large periodic side shell openings in global finite element models for evaluation of passenger ship hull girder static response in early design phase. The first technique is based on homogenization of side shell structure and modeling side shell openings with homogenized orthotropic material using 4-noded and 8-noded shell elements. Second technique is direct modeling of side shell openings using coarse mesh, where cost of simplification to geometry and mesh size is studied.

The proposed techniques are validated with respect to 3D fine mesh analysis in two cases. First, periodic side shell model is studied for evaluation of correct in plane response under uniform axial and shear loading. Second, the techniques are investigated in a box-like ship under 4-point bending load. Accuracy of both techniques is evaluated by means of hull girder deflection, longitudinal deck forces and side shell vertical shear forces. In addition, the performance in border of periodic grid and at areas of high strain gradients is investigated.

The results indicate that equivalent orthotropic modeling of both central and offset openings gives accurate global deflection and longitudinal bending response in a simple model where strain gradients are small. When significant strain gradients are introduced e.g. where internal longitudinal bulkheads are discontinuous, the deflection and longitudinal bending response accuracies are compromised. Local response of orthotropic model is less accurate and especially compromised at edges of periodic grid and areas of high strain gradient. Additional local errors arise due to micropolar behavior of offset openings, where the equivalence is only achieved in forces but not in moments due to application of classical theory of elasticity. No significant difference in response is observed whether 4- or 8-noded elements are applied.

For coarse mesh modeling a sensitivity analysis is performed taking account effect of simplification of structure and mesh size. A reasonable compromise between modeling effort, computational cost and accuracy is found at 4x4 elements per opening. Despite being stiffer in uniformly loaded periodic side shell model, the accuracy of coarse mesh modeling is shown to be reliable in application to box-like ship, where performance is not significantly affected by strain gradients and boundary effects.

Keywords: Cruise ship, finite element analysis, equivalent orthotropic modeling, coarse mesh modeling

TABLE OF FIGURES

Figure 1.1 Typical longitudinal stress distribution in mid-section [5].....	15
Figure 1.2 Ships global FE-model.....	15
Figure 1.3 Classification of subdomains, corner nodes (coarse global mesh), interface nodes and internal nodes [9].	17
Figure 1.4 Coarse modelling of openings [6].....	17
Figure 1.5 Homogenization of explicit structure to equivalent homogenized media.	18
Figure 1.6 Sub-modelling of periodic openings [5].	19
Figure 1.7 RVE deformation under pure shear load [17].	20
Figure 1.8 Sub-model with neighbouring structures constrained and loaded for derivation of equivalent shear stiffness [18].	21
Figure 1.9 2nd order computational homogenization principle [19].	22
Figure 1.10 Passenger ship side shell.	23
Figure 2.1. Plane rectangular bilinear element [10].....	25
Figure 2.2 Bilinear element (a). Bilinear element subject to bending moment M_1 (b). Explicit behaviour of plate subject to bending moment M_2 (c) [10].....	26
Figure 2.3 Quadratic quadrilateral element.	27
Figure 2.4 Alternative selections of unit cell in side shell [22].	28
Figure 2.5 Homogenization of stiffened panel with openings.	29
Figure 2.6 Deformation of homogenized RVE. Axial components (left), shear components (right).	33
Figure 2.7 RVE with central opening.	35
Figure 2.8 RVE with central opening for shear load case.	37
Figure 2.9 Model of 3x3 RVE-s under horizontal axial load.....	40
Figure 2.10 Model of 3x3 RVE-s under vertical axial load.	41
Figure 2.11 Submodel for vertical axial load case.	42
Figure 2.12 Model of 3x3 RVE-s under shear load.	44
Figure 2.13 RVE with offset opening and stiffeners for shear load case.	45
Figure 2.14 Force and moment on RVE with central opening under horizontal tension (heterogeneous explicit model - top, Homogeneous equivalent model - bottom).	46
Figure 2.15 Force and moment on RVE with offset opening under horizontal tension (heterogeneous explicit model - top, Homogeneous equivalent model - bottom).	47
Figure 2.16 Rectangular components of stress and couple-stress [24].	48

Figure 2.17 Boundary layer on ships side shell.	48
Figure 2.18 Antisymmetric deformation of unit cells under pure shear load (1F - top and 3F - bottom).	49
Figure 3.1 Section of global coarse mesh model.	51
Figure 3.2 Shear deformation components of an opening.	52
Figure 3.3 Simplification of balcony opening for coarse mesh modelling. a – explicit model, b – neglecting of corner radius, c – offsetting the opening to bottom of the panel and lumping stiffeners to side of the opening.	52
Figure 3.4 Local bending of vertical and horizontal plate strips under shear load. Explicit geometry - left, simplified model - right.	53
Figure 4.1 Central opening (left), typical offset balcony opening (right).	55
Figure 4.2 Fine mesh reference model of balcony opening. Offset – left, central – right.	57
Figure 4.3 Shear stiffness due to simplification of typical balcony opening (Figure 4.1). a) explicit. b) excluded corner radii. c) excluded corner radii, opening offset to bottom edge of plate and stiffeners lumped to opening edge.	58
Figure 4.4 Shear stiffness modelling accuracy of typical balcony opening.	59
Figure 4.5 Periodic side shell test model.	59
Figure 4.6 Submodel of 3x3 openings in side shell constrained and loaded for horizontal tension load case (left) and vertical tension load case (right).	60
Figure 4.7 Submodel of 3x3 openings in side shell constrained and loaded for shear load case.	61
Figure 4.8 Horizontal displacement curves along web frames under shear load.	61
Figure 4.9 Box ship model 1 (M1).	62
Figure 4.10 Box ship model 2 (M2).	63
Figure 4.11 4-point bending loads.	64
Figure 4.12 Example of fine, coarse and orthotropic mesh size for box-like ship.	64
Figure 4.13 Deflection curves along deck 0 - side shell intersection line, M1 central openings.	66
Figure 4.14. Deflection difference of coarse and orthotropic models compared to fine mesh, M1 central openings.	66
Figure 4.15 Longitudinal deck forces in region 2, M1 central openings.	67
Figure 4.16 Vertical shear forces in side shell, region 1, M2 central openings.	68
Figure 4.17 Deflection curves along deck 0 - side shell intersection line, M1 offset openings.	69
Figure 4.18 Longitudinal deck forces in region 2, M1 offset openings.	70
Figure 4.19 Moments M_y of in plane forces about mid-height of an opening, region 2 (mid-ship), M1 offset openings.	70
Figure 4.20 Vertical shear forces in side shell of box-like ship, region 1, M2 offset openings.	71

Figure 4.21 Explicit model of modified box-like ship model. Majority of shear flow, central openings.....72

Figure 4.22 Vertical shear forces in side shell of modified box ship, region 1, central openings.....73

Figure 4.23 Longitudinal force in decks of modified box ship, region 2, central openings.74

LIST OF TABLES

Table 4.1. Equivalent orthotropic properties of balcony openings.....	56
Table 4.2. Axial forces causing 1 mm displacement of vertical/horizontal side of side shell model.	60

NOMENCLATURE

Notations

E	Young's modulus	x, y, z	local coordinates
G	Shear modulus	u, v, w or $u_x,$ u_y, u_z	displacements in x-, y-, z- direction
ε	normal strain	L	height of RVE
γ	shear strain	b	breadth of RVE
κ	curvature	t	plate thickness
ν	Poisson's ratio	R	opening corner radius
F	force	S	area
M	moment	V	volume
U	strain energy	I	Second moment of area
W	external work	α	rotation about x-axis
σ	stress	β	rotation about y-axis
N_i	Shape function of node i		

Subscripts

x, y, z	local coordinates	b	bottom plate strip of RVE
o	window opening	t	top plate strip of RVE
top	refers to top edge of RVE	v	vertical plate strip of RVE
bot	refers to bottom edge of RVE		
left	refers to left edge of RVE		
right	refers to right edge of RVE		

Abbreviations

FE	Finite element
FEA	Finite element analysis
3D	Three dimensional
RVE	Representative volume element
DOF	Degree of freedom

1. INTRODUCTION

1.1 Background

Size and complexity of passenger ships has significantly increased over past decades. Late 1980's and early 1990's saw passenger ships of gross tonnage up to 75000 with notable examples of Sovereign [1] and Fantasy class [2]. In past ten years the size of cruise ships has reached a new peak with three Oasis class ships of 225 000 GT delivered to Royal Caribbean Cruise Line while operators such as Costa Cruises, Aida Cruises, MSC Cruises and Star Cruises have ordered ships around 200 000 GT area [3]. In addition to increase in size, the structure has become more complex due to demand for large open spaces, theatres, atriums, large balcony openings and split superstructures, which increase complexity of structural response. As a result, there is demand for tools that can be applied in structural analysis to explore possibility of innovative solutions.

Assessment of passenger ship global response is a challenging task as the hull girder response does not follow beam theory as bulk carriers and tankers do [4]. This is largely due to complex nature of force transfer between hull and superstructure but also a result of reduced in plane shear stiffness of side shell. The reduction in side shell shear stiffness is caused by side shell openings which results in sliding between decks and affects superstructure to carry longitudinal bending loads. The result is non-linear longitudinal stress distribution under longitudinal bending load [5] as shown on Figure 1.1. For this purpose, global 3D finite element analysis (FEA) is the most reliable method to examine structural behavior and only method considered sufficient for cruise ships as recognized by International Ships and Offshore Structures Congress in 1997 [6].

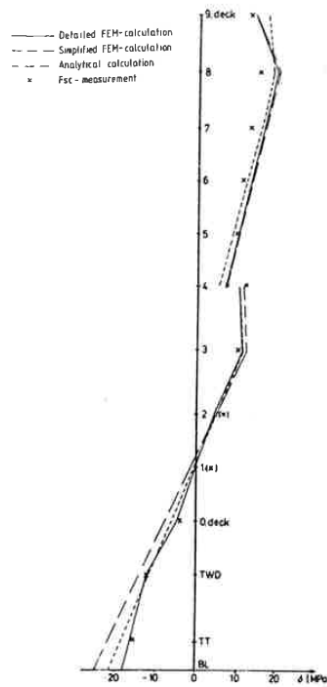


Figure 1.1 Typical longitudinal stress distribution in mid-section [5].

The basis of global strength assessment is the global finite element model of the ship as shown in Figure 1.2. Due to practical reasons of modelling effort and computational cost the global structure is modelled using coarse mesh where the element size is few meters – typically 1 or 2 elements per spacing of the web frames [6]. In global mesh only primary structural members i.e. plates, girders, web frames and pillars are modelled directly, while structures such as plates with cut-outs and stiffened panels are modelled either with simplified coarse mesh or as elements with equivalent properties. Proposed modeling techniques for stiffened panels provide accurate response [7] while modeling techniques for perforated side shell need further investigation.

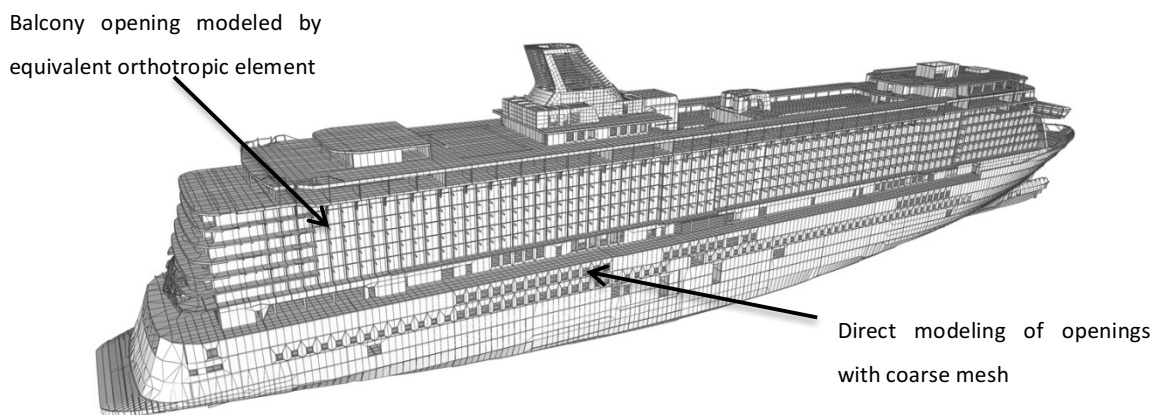


Figure 1.2 Ship's global FE-model.

For reliable global response, it is essential that the elements incorporating openings in side shell are modelled accurately since openings in plate significantly reduce in plane shear stiffness [5]. This is important to consider in structural analyses as reduced side shell shear stiffness affects efficiency of superstructure to carry vertical hull girder bending moment and shear force which affect global response.

1.2 State of the art

Global 3D finite element analysis with fine mesh is considered the most reliable method of assessing structural response of a ship [8]. However, modelling time of detailed fine mesh global model of a large ship is very time consuming. In addition, due to high computational cost the method is not applicable in early design phase of large and complex ships where design changes are significant. Therefore, several alternative approaches have been proposed in literature to obtain accurate structural response with lower cost than fine mesh modelling.

1.2.1 Domain decomposition method

In case of domain decomposition method, the finite element problem is not solved in one step but interface is formed between global coarse mesh and local fine mesh (rectangular plate with opening) problems. Classical domain decomposition consists of three steps. Firstly, local problem is solved on the fine scale of the detail to derive its homogenized behavior. Secondly, global model is solved to obtain global behavior of the structure. Thirdly, local solution at the detail level is obtained based on global behavior [9] [10]. Similar technique is applied in hierarchical Dirichlet projection method [11].

These methods however have two shortcomings. First, since the structure may not be periodic, assumptions are made on boundary conditions of detail level problem. Second, global coarse model results are used as boundary conditions to obtain solution at detail level – later may introduce artificial edge effect which may affect local stress calculations. Shortly, the problems at local and global scale are independent of each other [9].

These problems are overcome with use of FETI-DP algorithm [12], [13] in which interface constraints between detail level models are enforced by using Lagrange multiplier and corner degrees of freedom of interfaces are prescribed iteratively. The division of global model into domains with corner and interface nodes is presented on Figure 1.3. Overall the domain decomposition method is promising but further work is required to bring down the computational cost. It is suggested to use the method by applying fine mesh only to crucial areas while modelling the rest of structure with homogenized elements [9].

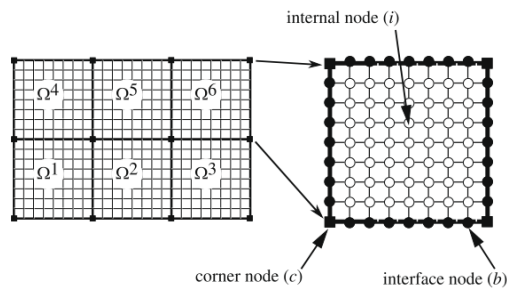


Figure 1.3 Classification of subdomains, corner nodes (coarse global mesh), interface nodes and internal nodes [9].

1.2.2 Direct modelling with coarse mesh

Direct modelling of openings with coarse mesh has been proposed in Lloyd's Register 2004 rules and in [6]. An example is shown in Figure 1.4.

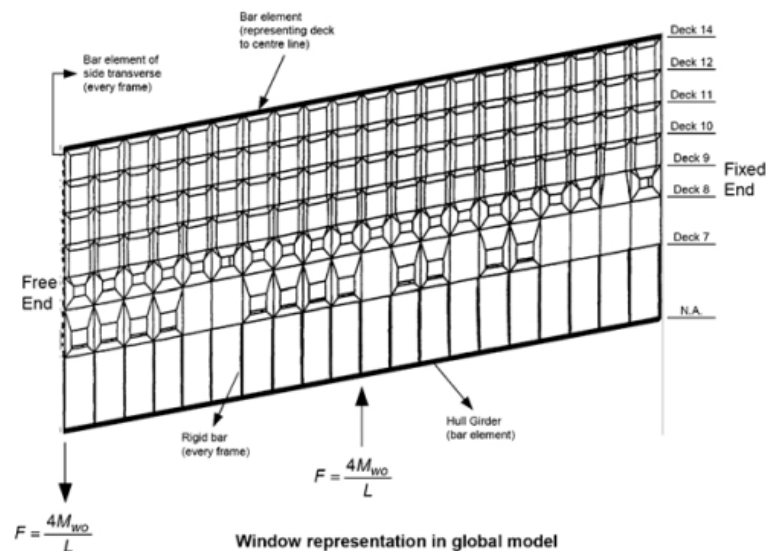


Figure 1.4 Coarse modelling of openings [6].

In this approach shear stiffness varies significantly with element size, shape and type [14]. The coarse mesh modeling accuracy has been studied for various opening sizes by Zanic et al. [6]. Modelling with 12 4-noded shell elements per web-frame/deck does not generally give satisfactory results and can be applied only for small openings ($\frac{L_o}{L} < 0,3; \frac{b_o}{b} < 0,3$). Accuracy can be increased by using 8-node shell elements. It is suggested that large openings are to be modelled with bracketed beam hybrid elements due to large number of 4-noded shell elements required for satisfactory accuracy [6]. Rounded corners of an opening can be taken into account with plate thickness correction factor curves obtained from FEA or by direct modelling [14].

In case of coarse mesh model with 1-2 plate elements per web frame length the opening deformation is uncoupled from deck deformation, thus stiffness of structure is underestimated. This however can be balanced with overestimation of opening stiffness due to coarse mesh [14].

Melk proposed to model balcony openings with Timoshenko beams representing plate strips between openings [15]. The modelling approach was proven accurate for given geometry but method suffers from fact that modelled unit cell is not located between consecutive web frames and decks. Therefore, local mesh refinement would be required around balcony openings.

1.2.3 Modelling with equivalent orthotropic elements

The principle in equivalent orthotropic modeling is that heterogeneous structure e.g perforated side shell with properties E, G, ν is replaced with homogeneous media with equivalent averaged properties E_x, E_y, G, ν . In this case representative volume element (RVE) of periodic structure is homogenized and replaced with equivalent element as illustrated on Figure 1.5.

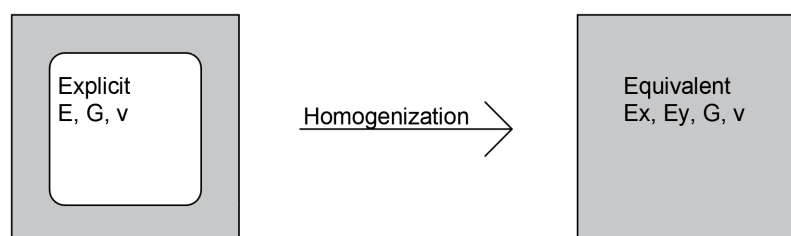


Figure 1.5 Homogenization of explicit structure to equivalent homogenized media.

Alternatively equivalence in stiffness can be realized by plate element with reduced thickness to satisfy shear stiffness equivalence and rod elements for compensation of axial stiffness [16], in this case equivalency in Poisson's ratio is not achieved.

Equivalent properties can be derived either analytically or by sub-modelling. Fransman has analytically derived equations for centrally placed rectangular window (Figure 1.6, middle) in grid of similar windows and window adjacent to rigid bulkhead with one side (Figure 1.6, bottom). Different equivalent properties are derived for same structure in different locations because realistic boundary conditions need to be taken account during derivation of equivalent properties as interface to boundaries is lost in coarse orthotropic model. Corner radii are not considered by Fransman, contribution of window frames is included in the approach. [5]

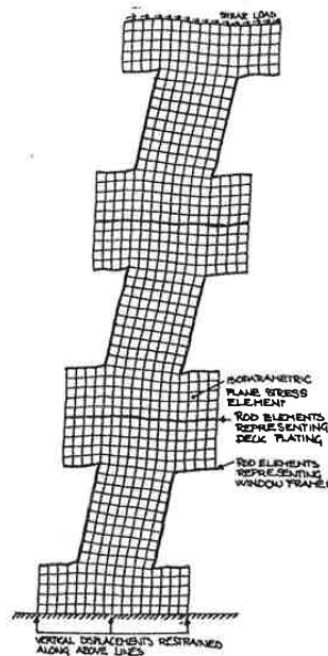


Figure 1.6 Sub-modelling of periodic openings [5].

Fricke et al. have derived analytical formula for shear stiffness of centrally placed rectangular window in a grid of similar windows. In addition, a formula for taking account corner radius is proposed. The formula requires calibration with finite element analysis [14].

Alternative option is to determine equivalent properties by sub-modelling. It has been determined that the deformation shape for plate with centrally placed hole in a grid of similar elements under uniform in plane shear load is anti-symmetric [17], [18]. Therefore, sub-model of single RVE is sufficient to obtain equivalent in plane properties of a plate with cut out. Anti-symmetric boundary conditions are given by equations 1.1-1.4 according to Figure 1.7.

Additionally, strains along edges of RVE are restricted according to equations 1.5-1.6. This has been determined to be natural deformation shape of RVE under uniform shear load by analysis of periodic grid under pure shear load by Sun [17] and confirmed in this thesis work. For offset openings, applicability of equations 1.5-1.6 has not been investigated and may result in overestimated shear stiffness.

$$v(-b, z) = v(b, z) \quad (1.1)$$

$$w(-b, z) = w(b, z) \quad (1.2)$$

$$v(y, -c) = v(y, c) \quad (1.3)$$

$$w(y, -c) = w(y, c) \quad (1.4)$$

$$\varepsilon_{zz}(\pm b, z) = 0 \quad (1.5)$$

$$\varepsilon_{yy}(y, \pm c) = 0 \quad (1.6)$$

The axial stiffness is obtained by analyzing the sub-model under uniaxial tension. In case of normal load in Y direction proposed boundary conditions are following [17]:

$$v(-b, z) = 0, \quad (1.7)$$

$$v(b, z) = const, \quad (1.8)$$

$$w(y, -c) = 0, \quad (1.9)$$

$$w(y, c) = const. \quad (1.10)$$

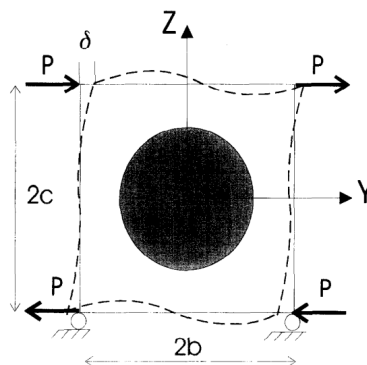


Figure 1.7 RVE deformation under pure shear load [17].

The shortcoming of this method is that these boundary conditions were derived only for centrally placed openings with no frames and stiffeners. Suitable boundary conditions for sub-modeling offset openings with stiffeners are proposed in chapter 2.3.3

The problem of offset openings is also tackled by modelling approach described by Amian [18]. It is based on a sub-model composed of an array of rectangular plates with openings and deriving equivalent properties based on response of plate inside a plate field as in Figure 1.8. The report does not however describe arising limitations due to modeling offset openings with homogeneous material, neither is contribution of stiffeners taken account. The accuracy of Amian’s modeling technique is not verified in global scale.



Figure 1.8 Sub-model with neighbouring structures constrained and loaded for derivation of equivalent shear stiffness [18].

1.2.4 Second order computational homogenization method

The basic principle of computational homogenization is illustrated on Figure 1.9. The macroscopic deformation gradient tensor \mathbf{F}_M and its gradient $\vec{\nabla}_0 \mathbf{F}_M$ obtained from macrostructure (global FE model) are transferred to microstructure in order to define boundary value problem on RVE. The problem on RVE is solved in standard way by FEA resulting boundary displacements and boundary surface tractions. By mathematical averaging equations, macroscopic stress tensor \mathbf{P}_M and higher order stress tensor ${}^3\mathbf{Q}_M$ are obtained. Tangent operators of stress and strain are obtained by

static condensation and fed back into macro scale problem. The nested finite element problems of macro (global) and micro (local) scale are solved iteratively [19].

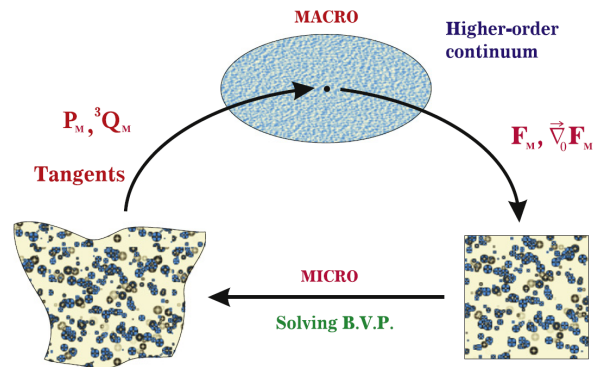


Figure 1.9 2nd order computational homogenization principle [19].

The advantage of second order computational homogenization method over classical homogenization method (and 1st order computational method), described in chapter 1.2.3, is accounting for large strain gradients (loading is not assumed uniform) and accurate modeling of edge effect [19]. The method is not however implemented into commercial FE solvers such as NX Nastran 11. Also, the computation and model preparation is costly compared to classical homogenization methods. This method is not applied in the thesis, but conclusions from related papers [19] and [20] are used to investigate and explain errors arising in classical homogenization method. These limitations have not received much attention in papers where classical homogenization method is applied to ships structures.

1.3 Aim of thesis

The aim of the thesis is to develop and implement modeling techniques for modeling ship's side shell openings such as window and balcony openings. The outcome will be an evaluation of modeling techniques which improves reliability and time consumption of static response assessment in early design phase. The technique should be computationally feasible and applicable in limited time frame of early design phase. The results will be validated with respect to response of box-like prismatic ship and side shell models according to 3D fine mesh FEA.

The assessment of modeling techniques is driven by typical modern passenger ship structure as in Figure 1.10. Various opening types are distinguished when considering applicability of different modeling techniques by opening type:

1. Balcony openings in a periodic grid of similar openings
2. Balcony openings in a periodic grid of similar openings with one edge free or next to rigid bulkhead
3. Balcony openings with irregular surroundings
4. Window openings in a periodic grid of similar openings with one edge free or next to rigid bulkhead
5. Hull openings with irregular surroundings

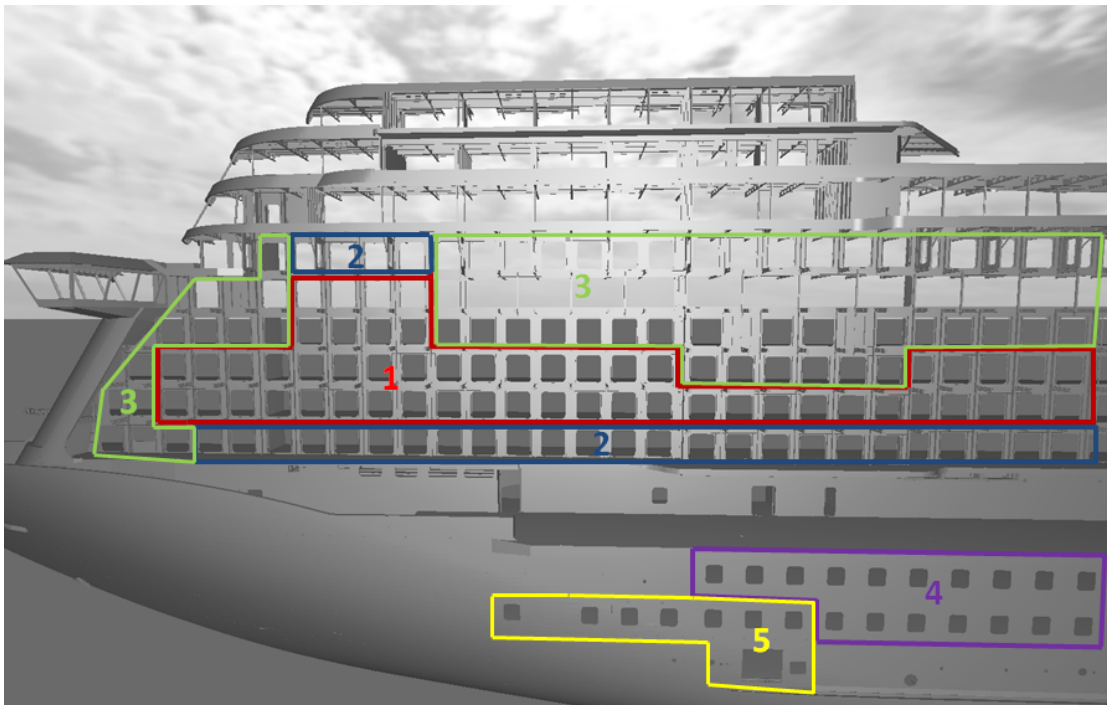


Figure 1.10 Passenger ship side shell.

Since homogenization is based on periodicity assumption the areas where periodicity is violated (3-5) are not considered. In this thesis, the applicability of modeling techniques for periodic type 1 openings and openings in edge of periodic structure (type 2) are studied. Equivalent orthotropic modelling is described in 2. Methods; explicit modeling with coarse mesh is discussed in 3. Direct modelling of openings with coarse mesh. The evaluation of each modeling approach is given in 4. Results. The evaluation of results and suggestions for modeling are presented in 5. Conclusions.

2. METHODS

2.1 Membrane finite elements for plane stress analysis

In following finite elements applied in the work are discussed in order to describe arising limitations due to discretization.

The properties of quadrilateral plane elements implemented in NX Nastran as CQUAD4 and CQUAD8 can be separated into membrane properties associated with plane displacements (u, v) and bending properties associated with out of plane displacements and rotations (w, α, β). Thus four-node quadrilateral plane element has 20 degrees of freedom [21]. The focus in this work is on in-plane properties, since these have a large effect on ships load carrying mechanism in global bending modes. Therefore, only membrane properties of the elements are discussed.

Plane rectangular bilinear element shown on Figure 2.1 has 8 degrees of freedom – u and v for each node. The displacement field according to nodal degrees of freedom is defined as

$$\begin{Bmatrix} u \\ v \end{Bmatrix} = \begin{bmatrix} N_1 & 0 & N_2 & 0 & N_3 & 0 & N_4 & 0 \\ 0 & N_1 & 0 & N_2 & 0 & N_3 & 0 & N_4 \end{bmatrix} \begin{Bmatrix} u_1 \\ v_1 \\ u_2 \\ v_2 \\ u_3 \\ v_3 \\ u_4 \\ v_4 \end{Bmatrix}, \quad (2.1)$$

where shape functions N_i are linear:

$$N_1 = \frac{1}{4ab}(a-x)(b-y), \quad (2.2)$$

$$N_2 = \frac{1}{4ab}(a+x)(b-y), \quad (2.3)$$

$$N_3 = \frac{1}{4ab}(a+x)(b+y), \quad (2.4)$$

$$N_4 = \frac{1}{4ab}(a-x)(b+y). \quad (2.5)$$

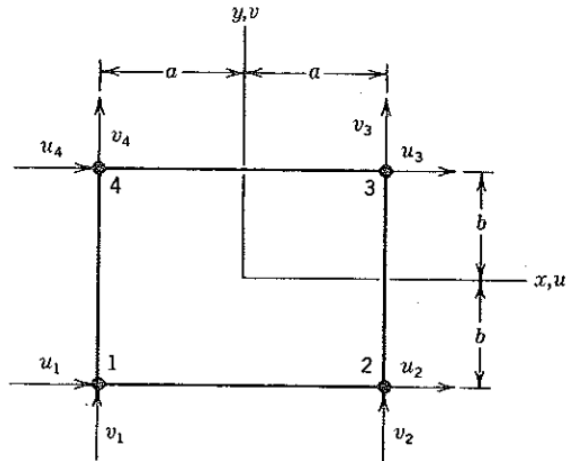


Figure 2.1. Plane rectangular bilinear element [10].

The strain displacement matrix $[B]$ is

$$[B] = \begin{bmatrix} \frac{\partial}{\partial x} & 0 \\ 0 & \frac{\partial}{\partial y} \\ \frac{\partial}{\partial y} & \frac{\partial}{\partial x} \end{bmatrix} [N] \quad (2.6)$$

and element stiffness matrix $[k]$ is

$$[k] = \int_{-b}^b \int_{-a}^a [B]^t [E] [B] t \, dx \, dy. \quad (2.7)$$

where $[E]$ is material property matrix.

Bilinear elements are attractive for their simple formulation but they are too stiff in bending. That is illustrated in Figure 2.2 (b) where bending moment M_1 is applied to rectangular bilinear element resulting in nodal displacements \bar{u} .

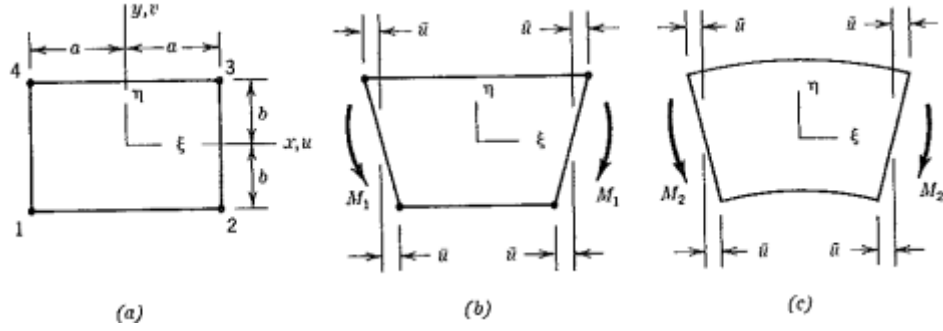


Figure 2.2 Bilinear element (a). Bilinear element subject to bending moment M_1 (b). Explicit behaviour of plate subject to bending moment M_2 (c) [10].

The displacement field of bilinear element under bending moment M_1 is found from

$$\begin{Bmatrix} u \\ v \end{Bmatrix} = \begin{bmatrix} N_1 & 0 & N_2 & 0 & N_3 & 0 & N_4 & 0 \\ 0 & N_1 & 0 & N_2 & 0 & N_3 & 0 & N_4 \end{bmatrix} \begin{Bmatrix} \bar{u} \\ 0 \\ -\bar{u} \\ 0 \\ \bar{u} \\ 0 \\ -\bar{u} \\ 0 \end{Bmatrix}. \quad (2.8)$$

The horizontal and vertical displacement field in bilinear element is obtained as:

$$u = \bar{u} \left(\frac{1}{4ab} (a-x)(b-y) - \frac{1}{4ab} (a+x)(b-y) + \frac{1}{4ab} (a+x)(b+y) - \frac{1}{4ab} (a-x)(b+y) \right) = \bar{u} \frac{xy}{ab}, \quad (2.9)$$

$$v = 0. \quad (2.10)$$

The correct displacements for membrane under pure in plane bending according to Figure 2.2 (c) are

$$u = \bar{u} \frac{xy}{ab} \quad \text{and} \quad v = \left(1 - \left(\frac{x}{a} \right)^2 \right) \frac{a\bar{u}}{2b} + \left(1 - \left(\frac{y}{b} \right)^2 \right) v \frac{b\bar{u}}{2a}. \quad (2.11)$$

By comparing displacement equations 2.9-2.11 it is found that while correct behavior results in storage of strain energy only due to normal strain, the behavior of bilinear element stores strain energy due to normal strains and shear strains. This results in too high bending stiffness of bilinear element [10].

By adding one node to each side of four-node quadrilateral a quadratic quadrilateral element (CQUAD8) as shown on Figure 2.3 is formed.

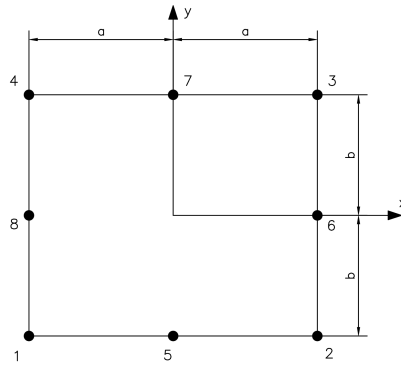


Figure 2.3 Quadratic quadrilateral element.

Shape functions for 8-noded element can be defined as

$$\begin{aligned}
 N_1 &= \frac{-1}{4ab}(a-x)(b-y)\left(1+\frac{x}{a}+\frac{y}{b}\right), \\
 N_2 &= \frac{-1}{4ab}(a+x)(b-y)\left(1-\frac{x}{a}+\frac{y}{b}\right), \\
 N_3 &= \frac{-1}{4ab}(a+x)(b+y)\left(1-\frac{x}{a}-\frac{y}{b}\right), \\
 N_4 &= \frac{-1}{4ab}(a-x)(b+y)\left(1-\frac{x}{a}-\frac{y}{b}\right), \\
 N_5 &= \frac{1}{2a^2b}(a-x)(b-y)(a+x), \\
 N_6 &= \frac{1}{2b^2a}(a+x)(b-y)(b+y), \\
 N_7 &= \frac{1}{2a^2b}(a-x)(b+y)(a+x), \\
 N_8 &= \frac{1}{2b^2a}(a-x)(b-y)(b+y).
 \end{aligned} \tag{2.12}$$

As a result of parabolic shape functions the deformation shape for 8-node element can take quadratic form and parasitic shear phenomenon can be avoided. In addition, the shear and axial forces on opposite edges of an element no longer need to be equal as for bilinear quadrilateral element [10].

2.2. Equivalent orthotropic material modeling

The principle in equivalent orthotropic modelling is that each single panel with opening between decks and web frames is modelled with one or more elements with equivalent stiffness properties. The representative volume element (RVE) is smallest volume from which equivalent properties can be derived. In periodic structure RVE can be chosen as unit cell of structure. There are several approaches in choosing the unit cell for which the equivalent properties are derived as shown on Figure 2.4. In this work, the third option is chosen as it naturally complies with global FE mesh, web frame and deck locations. In following only equivalent in plane properties are considered.

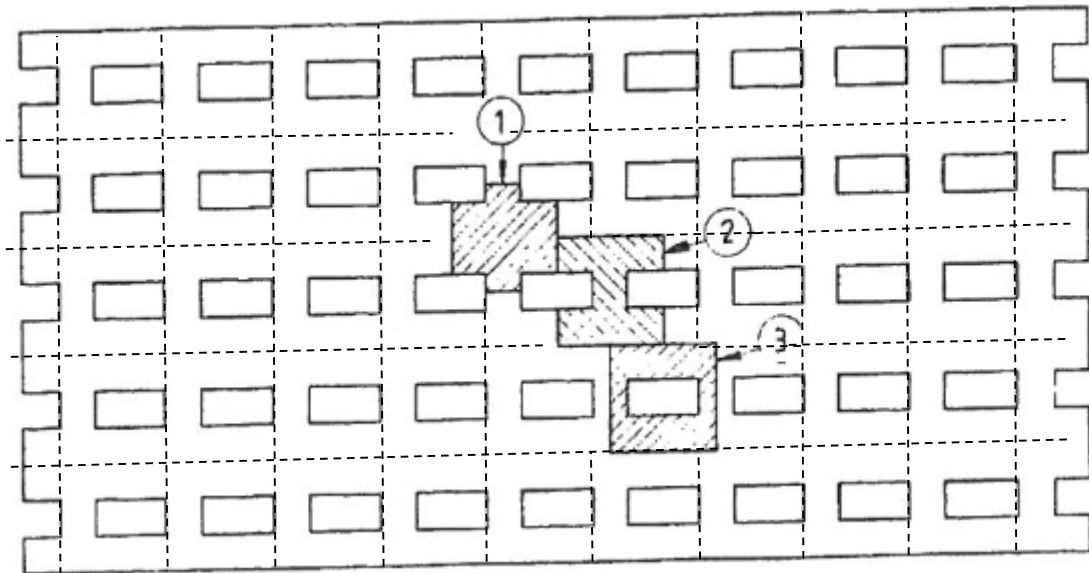


Figure 2.4 Alternative selections of unit cell in side shell [22].

The equivalent stiffness of heterogeneous structure is described by equivalent elements where homogenized in plane stiffness properties of explicit structure are considered. For homogenized model, a single layer shell element with same thickness as side shell plate is used. In case of stiffened openings, effective in plane stiffness of both plate with opening and stiffeners contribution are derived for this single layer equivalent material as illustrated in Figure 2.5. In homogenization, this means that all forces (plate and stiffener) on the boundaries of RVE are assumed to be in plate layer when calculating average stresses on boundaries of RVE.

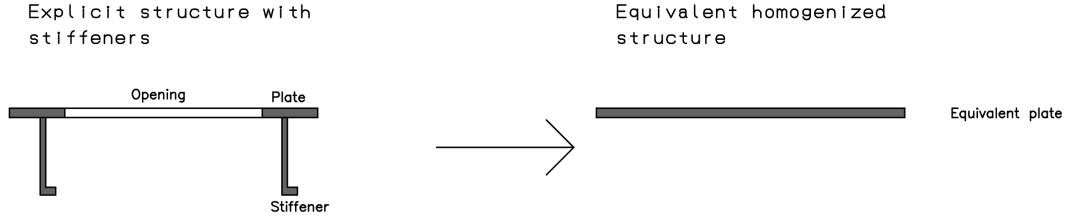


Figure 2.5 Homogenization of stiffened panel with openings.

Equivalent in-plane stiffness is set by 2D elasticity matrix $[E]_{eq}$ obtained according to principles described in chapter 2.3:

$$[E]_{eq} = \frac{1}{1 - \nu_{yx}\nu_{xy}} \begin{bmatrix} E_x & \nu_{yx}E_x & 0 \\ \nu_{xy}E_y & E_y & 0 \\ 0 & 0 & G(1 - \nu_{yx}\nu_{xy}) \end{bmatrix}. \quad (2.13)$$

2.2.1 Equivalent orthotropic element internal forces and strains relation

The normal stress vector $\{\sigma\} = \{\sigma_x \sigma_y \tau_{xy}\}$ is found by multiplying the strains $\{\varepsilon\} = \{\varepsilon_x \varepsilon_y \gamma_{xy}\}$ with the elasticity matrix $[E]_{eq}$:

$$\{\sigma\} = [E]_{eq}\{\varepsilon\}. \quad (2.14)$$

Internal forces in the in the membrane element are related to the in-plane stresses and deformations and they are obtained by integrating equation 2.14 over the plate thickness t . Thus, the normal force vector $\{N\} = \{N_x N_y N_{xy}\}^T$ is:

$$\{N\} = \int_{-t/2}^{t/2} [E]_{eq} \{\varepsilon\} dz. \quad (2.15)$$

Since membrane-bending coupling effects are neglected, the normal force can be written as:

$$\{N\} = [A]\{\varepsilon\}^0, \quad (2.16)$$

where $\{\varepsilon\}^0$ is the mid-plane strain vector

$$\begin{Bmatrix} \varepsilon_x^0 \\ \varepsilon_y^0 \\ \gamma_{xy}^0 \end{Bmatrix} = \begin{Bmatrix} \partial u_0 / \partial x \\ \partial v_0 / \partial y \\ \partial u_0 / \partial y + \partial v_0 / \partial x \end{Bmatrix}. \quad (2.17)$$

and $[A]$ is the membrane stiffness matrix:

$$[A] = \int_{-t/2}^{t/2} [E]_{eq} dz. \quad (2.18)$$

2.3 Homogenization

2.3.1 Equivalent stress, strain and strain energy

When modeling large periodic structure using RVE it is important to understand how it deforms when uniform tensile or shear load is applied at boundaries of the structure. In case of homogenous material, a uniform stress and strain state exists under uniform loading, but this is not the case in periodic structure which consists of openings surrounded by vertical and horizontal plate strips. Due to all RVE-s being identical they have identical stress and strain fields. Therefore, from global point of view the stress and strain fields are periodic except for narrow boundary layer (typically depth of 1 RVE) where the structure is loaded. The periodicity constraints obtained from large periodic structure are applied for single RVE to derive equivalent orthotropic properties from axial and shear load cases [17].

In classical homogenization theory, the structure is modeled as a homogenous orthotropic medium with effective elastic properties that describe averaged properties of the heterogeneous structure. For description of macroscopically homogenous medium the macro stress and strain are obtained by averaging stress and strain tensors over the volume of RVE [17]:

$$\bar{\sigma}_{ij} = \frac{1}{V} \int_V \sigma_{ij}(x, y, z) dV \quad (2.19)$$

and

$$\bar{\varepsilon}_{ij} = \frac{1}{V} \int_V \varepsilon_{ij}(x, y, z) dV. \quad (2.20)$$

For equivalence between actual heterogeneous structure and homogenous medium strain energy equivalence is used. Total strain energy U stored in volume V of equivalent medium is:

$$U = \frac{1}{2} \bar{\sigma}_{ij} \bar{\varepsilon}_{ij} V \quad (2.21)$$

The strain energy stored in heterogeneous RVE is

$$\begin{aligned} U' &= \int_V \frac{1}{2} \sigma_{ij} \varepsilon_{ij} dV = \frac{1}{2} \int_V \sigma_{ij} (\varepsilon_{ij} - \bar{\varepsilon}_{ij} + \bar{\varepsilon}_{ij}) dV \\ &= \frac{1}{2} \int_V \sigma_{ij} (\varepsilon_{ij} - \bar{\varepsilon}_{ij}) dV + \frac{1}{2} \bar{\varepsilon}_{ij} \int_V \sigma_{ij} dV \\ &= \frac{1}{2} \int_V \sigma_{ij} (\varepsilon_{ij} - \bar{\varepsilon}_{ij}) dV + \frac{1}{2} \bar{\sigma}_{ij} \bar{\varepsilon}_{ij} V \end{aligned} \quad (2.22)$$

Therefore

$$\begin{aligned} U' - U &= \frac{1}{2} \int_V \sigma_{ij} (\varepsilon_{ij} - \bar{\varepsilon}_{ij}) dV \\ &= \frac{1}{2} \int_V \sigma_{ij} \left(\frac{\partial}{\partial x_j} u_i - \frac{\partial}{\partial x_j} \bar{u}_i \right) dV \end{aligned} \quad (2.23)$$

According to classical theory of elasticity, equilibrium equation $\frac{\partial \sigma_{ij}}{\partial x_j} = 0$ due to absence of volume forces and

$$U' - U = \frac{1}{2} \int_V \frac{\partial}{\partial x_j} (\sigma_{ij} (u_i - \bar{u}_i)) dV \quad (2.24)$$

According to Gauss theorem, the volume integral can be converted to surface integral

$$U' - U = \frac{1}{2} \int_S \sigma_{ij} (u_i - \bar{u}_i) n_j dS, \quad (2.25)$$

where S is surface of RVE and n_j outward normal of the surface. On the surface S

$$u_i = \bar{u}_i \quad (2.26)$$

Therefore

$$U' = U \quad (2.27)$$

In more general case when deformation shape of RVE is antisymmetric ($u_{y,top} - u_{y,bot} = \text{const} = \bar{u}_y$, $u_{x,right} - u_{x,left} = \text{const} = \bar{u}_x$, $u_{x,top} - u_{x,bot} = \text{const} = \bar{u}_x$ and $u_{y,right} - u_{y,left} = \text{const} = \bar{u}_y$) and stress field on RVE is symmetric ($\sigma_{ij,top} = \sigma_{ij,bot}$ and $\sigma_{ij,left} = \sigma_{ij,right}$), the strain energy equilibrium according to deformation of homogenized RVE presented on Figure 2.6 is:

$$\begin{aligned}
U' - U &= \frac{1}{2} \int_S \sigma_{ij} (u_i - \bar{u}_i) n_j dS = \\
&= \frac{1}{2} \int_{S_{bot}} \sigma_{yy,top} (u_{y,bot} - 0) (-n_y(x)) dS \\
&+ \frac{1}{2} \int_{S_{top}} \sigma_{yy,top} (u_{y,top} - \bar{u}_y) (n_y(x)) dS \\
&+ \frac{1}{2} \int_{S_{left}} \sigma_{xx,left} (u_{x,left} - 0) (-n_x(y)) dS \\
&+ \frac{1}{2} \int_{S_{right}} \sigma_{xx,left} (u_{x,right} - \bar{u}_x) (n_x(y)) dS \quad (2.28) \\
&+ \frac{1}{2} \int_{S_{bot}} \sigma_{xy,top} (u_{x,bot} - 0) (-n_y(x)) dS \\
&+ \frac{1}{2} \int_{S_{top}} \sigma_{xy,top} (u_{x,top} - \bar{u}_x) (n_y(x)) dS \\
&+ \frac{1}{2} \int_{S_{left}} \sigma_{xy,left} (u_{y,left} - 0) (-n_x(y)) dS \\
&+ \frac{1}{2} \int_{S_{right}} \sigma_{xy,left} (u_{y,right} - \bar{u}_y) (n_x(y)) dS =
\end{aligned}$$

$$\begin{aligned}
&= [\text{considering that } S_{top} = S_{bot} \text{ and } S_{left} = S_{right}] \\
&= \frac{1}{2} \int_{S_{bot}} \sigma_{yy,top} (-u_{y,bot} + u_{y,top} - \bar{u}_y) n_y(x) dS \\
&+ \frac{1}{2} \int_{S_{left}} \sigma_{xx,left} (-u_{x,left} + u_{x,right} - \bar{u}_x) n_x(y) dS \\
&+ \frac{1}{2} \int_{S_{bot}} \sigma_{xy,top} (-u_{x,bot} + u_{x,top} - \bar{u}_x) n_y(x) dS \\
&+ \frac{1}{2} \int_{S_{left}} \sigma_{xy,left} (-u_{y,left} + u_{y,right} - \bar{u}_y) n_x(y) dS = 0,
\end{aligned} \tag{2.28}$$

where surface normals n_x and n_y were assumed equal for heterogeneous and homogeneous structures as the change of surface normal due to deformation is very small.

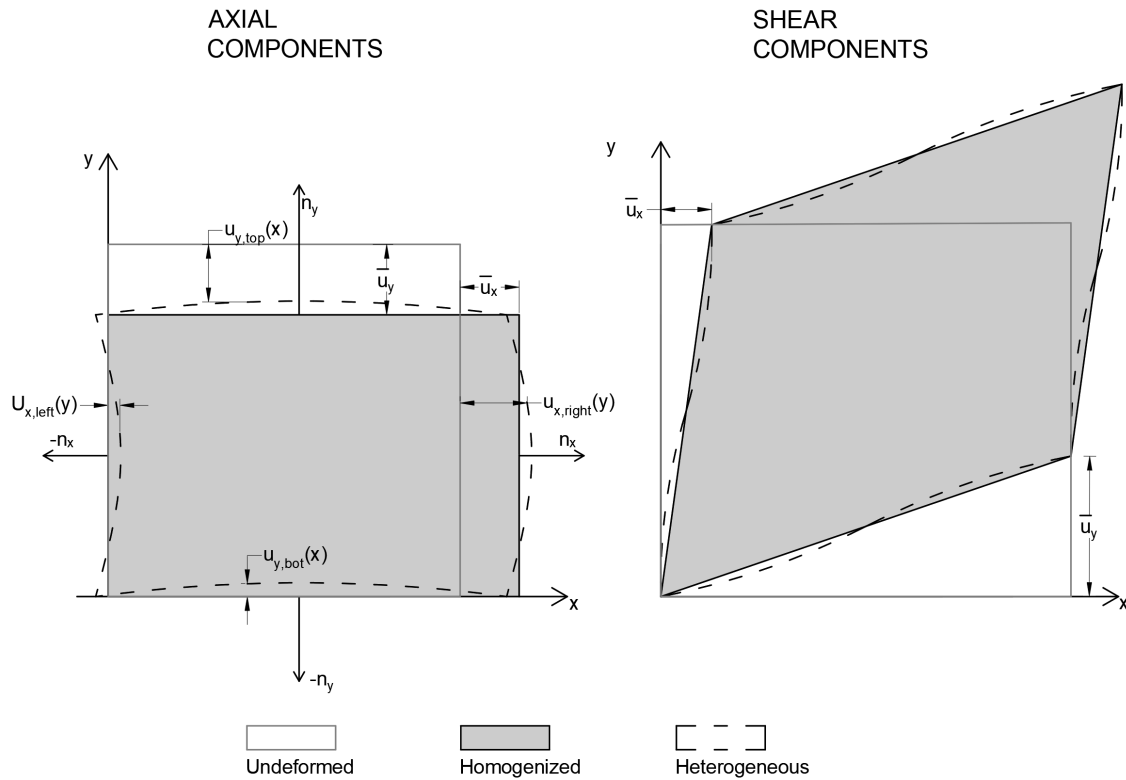


Figure 2.6 Deformation of homogenized RVE. Axial components (left), shear components (right).

Thus, the average stress $\bar{\sigma}_{ij}$ and strain $\bar{\epsilon}_{ij}$ fulfill equivalence in strain energy between explicit heterogeneous material and equivalent homogeneous material. These average expressions are used for derivation of heterogeneous structure's equivalent properties. The stress and strain state

of heterogeneous structure is obtained by FEA. For simpler analysis, the volume integral of strain field can be expressed in form of surface integral

$$\bar{\varepsilon}_{ij} = \frac{1}{V} \int_V \varepsilon_{ij}(x, y, z) dV = \frac{1}{2V} \int_S (u_i n_j + u_j n_i) dS \quad (2.29)$$

where S is the boundary surface of RVE, u_i is i -component of displacement and n_j is j -component normal to S [17].

2.3.2 Homogenization of orthotropic RVE with central opening

In case of panels with central opening and no stiffeners orthotropic properties are valid for equivalent elements as shown in [17]. According to definition, an orthotropic material has minimum of 2 orthogonal planes of symmetry where elastic properties are independent of direction in each plane. Thus, their constitutive matrices are composed of 9 independent variables. The conventional compliance matrix is in form of

$$\begin{bmatrix} \varepsilon_{xx} \\ \varepsilon_{yy} \\ \varepsilon_{zz} \\ \varepsilon_{yz} \\ \varepsilon_{zx} \\ \varepsilon_{xy} \end{bmatrix} = \begin{bmatrix} \frac{1}{E_x} & -\frac{\nu_{yx}}{E_y} & -\frac{\nu_{zx}}{E_z} & 0 & 0 & 0 \\ -\frac{\nu_{xy}}{E_x} & \frac{1}{E_y} & -\frac{\nu_{zy}}{E_z} & 0 & 0 & 0 \\ -\frac{\nu_{xz}}{E_x} & -\frac{\nu_{yz}}{E_y} & \frac{1}{E_z} & 0 & 0 & 0 \\ 0 & 0 & 0 & \frac{1}{2G_{yz}} & 0 & 0 \\ 0 & 0 & 0 & 0 & \frac{1}{2G_{zx}} & 0 \\ 0 & 0 & 0 & 0 & 0 & \frac{1}{2G_{xy}} \end{bmatrix} \begin{bmatrix} \sigma_{xx} \\ \sigma_{yy} \\ \sigma_{zz} \\ \sigma_{yz} \\ \sigma_{zx} \\ \sigma_{xy} \end{bmatrix}, \quad (2.30)$$

where $\frac{\nu_{yx}}{E_y} = \frac{\nu_{xy}}{E_x}$, $\frac{\nu_{zx}}{E_z} = \frac{\nu_{xz}}{E_x}$, $\frac{\nu_{zy}}{E_y} = \frac{\nu_{yz}}{E_z}$.

In case of 2-dimensional membrane problems on x - y plane the compliance matrix takes the form

$$\begin{bmatrix} \varepsilon_{xx} \\ \varepsilon_{yy} \\ \varepsilon_{xy} \end{bmatrix} = \begin{bmatrix} \frac{1}{E_x} & -\frac{\nu_{yx}}{E_y} & 0 \\ -\frac{\nu_{xy}}{E_x} & \frac{1}{E_y} & 0 \\ 0 & 0 & \frac{1}{2G_{xy}} \end{bmatrix} \begin{bmatrix} \sigma_{xx} \\ \sigma_{yy} \\ \sigma_{xy} \end{bmatrix}, \quad (2.31)$$

where $\frac{\nu_{yx}}{E_y} = \frac{\nu_{xy}}{E_x}$.

Therefore, for of equivalency between explicit heterogeneous structure and homogenized equivalent media effective E_x , E_y , G_{xy} , and ν_{xy} need to be determined [17].

EFFECTIVE MODULI

The RVE for analysis of normal loads is given in Figure 2.7. In case of axial loading the boundaries of RVE correspond to symmetry lines of RVE.

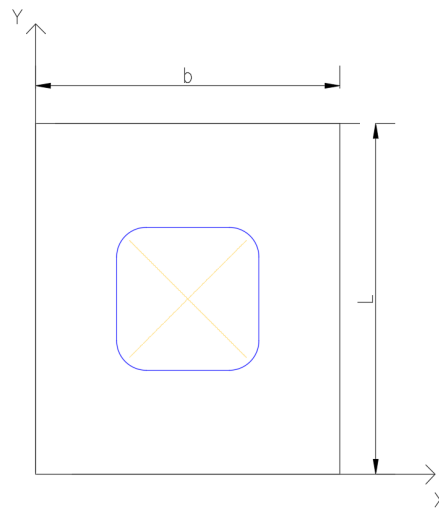


Figure 2.7 RVE with central opening.

The normal displacements of the boundary cause the boundary to displace only parallel to the original one. The displacement constraints, according to equations 1.7-1.10 are applicable to heterogeneous FE model of RVE:

$$u(0, y) = 0$$

$$u(b, y) = \text{const} = \delta_x \quad (2.32)$$

$$v(x, 0) = 0$$

$$v(x, L) = \text{const} = \delta_y,$$

where u and v are displacements in x and y direction respectively. The displacements δ_x and δ_y are obtained from finite element analysis of RVE.

The horizontal axial loading is modelled by forced displacement δ_x on side $x = b$. The force F_x is obtained as interface load acting on side $x = b$. Axial average strain can be expressed as

$$\bar{\varepsilon}_{xx} = \frac{1}{2V} \int_S (u_x n_x + u_x n_x) dS = \frac{1}{V} \int_S u_x n_x dS = \frac{\delta_x}{b}. \quad (2.33)$$

The strain energy absorbed is

$$U = \frac{1}{2} \bar{\sigma}_{ij} \bar{\varepsilon}_{ij} V = \frac{1}{2} \bar{\sigma}_{xx} \bar{\varepsilon}_{xx} V + \frac{1}{2} \bar{\sigma}_{yy} \bar{\varepsilon}_{yy} V + \frac{1}{2} \bar{\sigma}_{xy} \bar{\varepsilon}_{xy} V = \frac{1}{2} \bar{\sigma}_{xx} \bar{\varepsilon}_{xx} V \quad (2.34)$$

since $\bar{\sigma}_{yy} \bar{\varepsilon}_{yy} = 0$ and $\bar{\sigma}_{xy} \bar{\varepsilon}_{xy} = 0$ as determined from finite element analysis of RVE. The average stresses $\bar{\sigma}_{yy}$ and $\bar{\sigma}_{xy}$ are zero on each side of RVE despite σ_{yy} being locally non-zero. $\bar{\varepsilon}_{yy} \neq 0$ while $\bar{\varepsilon}_{xy} = 0$, therefore the strain energy is absorbed only due to horizontal stress $\bar{\sigma}_{xx}$ and strain $\bar{\varepsilon}_{xx}$.

The external work W which equals strain energy absorbed is

$$W = \frac{1}{2} F_x \delta_x = \frac{1}{2} \bar{\sigma}_{xx} \bar{\varepsilon}_{xx} V = \frac{1}{2} \bar{\sigma}_{xx} \frac{\delta_x}{b} V. \quad (2.35)$$

Thus

$$\bar{\sigma}_{xx} = \frac{F_x}{Lt} \quad (2.36)$$

where t is thickness of the RVE. The equivalent longitudinal modulus and Poisson's ratio are obtained from

$$E_x = \frac{\bar{\sigma}_{xx}}{\bar{\varepsilon}_{xx}} = \frac{F_x b}{Lt \delta_x} \text{ and } \nu_{xy} = -\frac{\bar{\varepsilon}_{yy}}{\bar{\varepsilon}_{xx}} = -\frac{\delta_y b}{\delta_x L}. \quad (2.37)$$

Similarly, for vertical tension case, forced displacement applied for boundary $y = L$ yields

$$E_y = \frac{\bar{\sigma}_{yy}}{\bar{\varepsilon}_{yy}} = \frac{F_y L}{bt \delta_y}, \quad \nu_{yx} = -\frac{\bar{\varepsilon}_{xx}}{\bar{\varepsilon}_{yy}} = -\frac{\delta_x L}{\delta_y b} \text{ or } \nu_{yx} = \frac{\nu_{xy}}{E_x} E_y. \quad (2.38)$$

In case of shear loading the deformed shape of RVE needs to satisfy periodicity and symmetry conditions. In general, large repetitive structure need to be analysed to obtain natural boundary conditions for single RVE. However, it was tested that analysis of 3x3 RVE-s is sufficient to establish accurate boundary conditions for single RVE under pure shear load. The natural displacement field and boundary conditions for RVE under pure shear load are obtained from central RVE as it is sufficiently removed from boundaries. Following boundary conditions for sub-modelling shear load case are proposed for RVE shown on Figure 2.8:

$$\begin{aligned}
 u(0, y) &= u(b, y) \\
 v(0, y) &= v(b, y) \\
 u(x, 0) &= u(x, L) \\
 v(x, 0) &= v(x, L) \\
 \varepsilon_{xx}(x, 0) = \varepsilon_{xx}(x, L) = 0 \text{ or } u(x, 0) = u(x, L) = \delta_x \\
 \varepsilon_{yy}(0, y) = \varepsilon_{yy}(b, y) = 0 \text{ or } v(0, y) = v(b, y) = \delta_y
 \end{aligned}
 \tag{2.39}$$

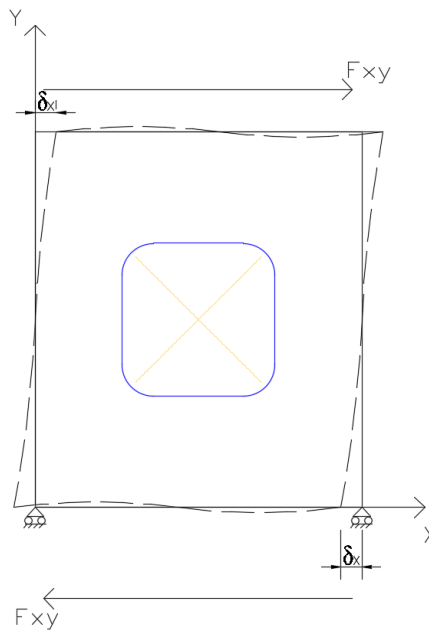


Figure 2.8 RVE with central opening for shear load case.

For application of shear load case equal and opposite shear loads F_{xy} are applied on edges $y = 0$ and $y = L$. The RVE is placed on rollers to eliminate rigid body motion ($\delta_y = 0$). The vertical reaction from rollers and constraint $\varepsilon_{yy}(0, y) = \varepsilon_{yy}(b, y) = 0$ result in effective shear force on

vertical sides or RVE, thus both vertical and horizontal shear components are active and RVE is under pure shear load. Average in plane shear strain is obtained from

$$\begin{aligned}\bar{\gamma}_{xy} &= \frac{2}{V} \int_V \varepsilon_{xy} dV \\ &= \frac{1}{V} \int_S (u_x n_y + u_y n_x) dS =\end{aligned}\quad (2.40)$$

$$\frac{2\delta_x}{L}.$$

Form external work - strain energy equilibrium

$$\frac{1}{2} F_{xy} 2\delta_x = \frac{1}{2} \bar{\sigma}_{xy} \bar{\gamma}_{xy} V = \frac{1}{2} \bar{\sigma}_{xy} \frac{2\delta_x}{L} Lbt = \bar{\sigma}_{xy} \delta_x bt \quad (2.41)$$

$$\bar{\sigma}_{xy} = \frac{F_{xy}}{bt} \quad (2.42)$$

The effective in plane shear modulus is found as

$$G_{xy} = \frac{\bar{\sigma}_{xy}}{\bar{\gamma}_{xy}} = \frac{F_{xy} L}{bt 2\delta_x}, \quad (2.43)$$

where $2\delta_x$ is horizontal displacement of edge $y = L$ relative to edge $y = 0$.

2.3.3 Homogenization of RVE with offset openings and stiffeners

In ship's global models the equivalent mesh is organized so that there are few equivalent elements between web frames and decks. The preferred mesh size of side shell is usually 1 or 2 elements per web frame spacing and 1 element between decks. The location of RVE needs to coincide with global mesh arrangement so that accurate equivalent property can be applied for every equivalent element. In case of balconies, the opening is usually not in the center of RVE and stiffeners are included in the structure, therefore homogenization of structure with offset openings and stiffeners is investigated.

For equivalent orthotropic modeling described above, the terms C13 and C23 in equation 2.44 [18] which quantify the coupling between shear and axial response were zero. In following the

presence of these coupling terms are determined for stiffened RVE with offset opening and suitable boundary conditions for analysis of RVE are established.

$$\begin{bmatrix} \varepsilon_{xx} \\ \varepsilon_{yy} \\ \varepsilon_{xy} \end{bmatrix} = \begin{bmatrix} \frac{1}{E_x} & -\frac{\nu_{yx}}{E_y} & C13 \\ -\frac{\nu_{xy}}{E_x} & \frac{1}{E_y} & C23 \\ C31 & C32 & \frac{1}{2G_{xy}} \end{bmatrix} \begin{bmatrix} \sigma_{xx} \\ \sigma_{yy} \\ \sigma_{xy} \end{bmatrix} \quad (2.44)$$

The equivalent in plane properties for stiffened panels with opening are derived for equivalent element with same thickness as explicit structure's plate layer. Therefore, contribution of stiffeners to equivalent properties are included in this single layer. In following all traction forces on RVE are assumed to be in plate layer when calculating averaged stresses. This is necessary to achieve equivalence between explicit and homogenized structure's in plane stiffness.

EFFECTIVE MODULI

The coupling terms can be determined from axial load cases. Since the opening is not in the centre of the RVE, the constraints proposed in chapter 2.3.2 are not valid. For horizontal axial load case, same constraints as for RVE with central opening can be applied for vertical edges due to symmetry with respect to vertical axis:

$$u(0, y) = 0 \quad (2.45)$$

$$u(b, y) = \text{const} = \delta_x.$$

The constraints of horizontal edges need to satisfy periodicity of the repetitive structure as well as its natural deformation field which occurs when uniform axial load is applied far from considered RVE. Following constraint equations for horizontal edges of RVE are proposed according to analysis of structure on Figure 2.9 consisting of 3x3 RVEs:

$$u(x, 0) = u(x, L) \quad (2.46)$$

$$v(x, L) - v(x, 0) = \text{const} = \delta_y.$$

The difference compared to central opening case is that horizontal edges of RVE no longer remain straight but their vertical displacements v and horizontal displacements u are coupled.

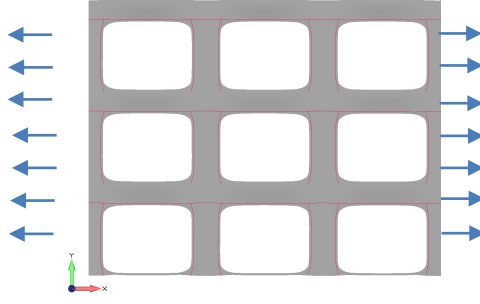


Figure 2.9 Model of 3x3 RVE-s under horizontal axial load.

In addition to in plane constraints, web frame and deck lines are constrained for out of plane displacement TZ and rotations RX, RY. These degrees of freedom are restricted in ship structures by decks and web frames which are not included in sub-modelling. The out of plane constraints are applied for analysis of all load cases: horizontal axial, vertical axial and shear.

The horizontal axial loading is modelled by forced displacement δ_x on side $x = b$. The force F_x is obtained as interface load acting on side $x = b$. The axial average strains can be expressed as

$$\bar{\epsilon}_{xx} = \frac{1}{2V} \int_S (u_x n_x + u_x n_x) dS = \quad (2.47)$$

$$\frac{1}{V} \int_S u_x n_x dS = \frac{\delta_x}{b},$$

$$\bar{\epsilon}_{yy} = \frac{1}{2V} \int_S (u_y n_y + u_y n_y) dS = \frac{1}{V} \int_S u_y n_y dS = \frac{1}{V} \int_L (u_{y,top} - u_{y,bottom}) t dL = \quad (2.48)$$

$$= \frac{1}{Lbt} tb \delta_y = \frac{\delta_y}{L}.$$

The average horizontal stress in RVE is obtained same as in chapter 2.3.2:

$$\bar{\sigma}_{xx} = \frac{F_x}{Lt}. \quad (2.49)$$

Equivalent properties can be obtained according to compliance matrix (2.44) from:

$$\bar{\epsilon}_{xx} = \frac{1}{E_x} \bar{\sigma}_{xx} - \frac{\nu_{yx}}{E_y} \bar{\sigma}_{yy} + C13 \bar{\sigma}_{xy}; \quad (2.50)$$

$$\bar{\epsilon}_{xy} = C31 \bar{\sigma}_{xx} + C32 \bar{\sigma}_{yy} + \frac{1}{2G_{xy}} \bar{\sigma}_{xy}. \quad (2.51)$$

From analysis of the RVE $\bar{\sigma}_{yy} = 0$, $\bar{\sigma}_{xy} = 0$ and $\bar{\varepsilon}_{xy} = 0$, thus

$$E_x = \frac{\bar{\sigma}_{xx}}{\bar{\varepsilon}_{xx}} = \frac{F_x b}{L t \delta_x} \text{ and } \nu_{xy} = -\frac{\bar{\varepsilon}_{yy}}{\bar{\varepsilon}_{xx}} = -\frac{\delta_y b}{\delta_x L} \quad (2.52)$$

and

$$\bar{\varepsilon}_{xy} = C_{13} \bar{\sigma}_{xx} \Rightarrow C_{13} = \frac{\bar{\varepsilon}_{xy}}{\bar{\sigma}_{xx}} = 0. \quad (2.53)$$

Therefore, there is no coupling between horizontal normal and shear term.

For vertical axial load case, same constraints as for RVE with central opening can be applied for vertical edges due to symmetry with respect to vertical axis. The boundary constraints for horizontal edges $y=L$ and $y=0$ were established by analysing displacement field of a structure of 3x3 openings under vertical tension, Figure 2.10.

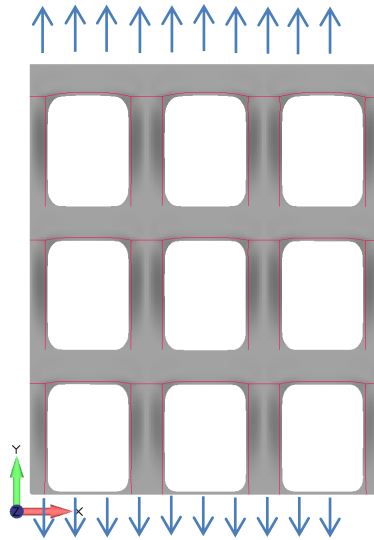


Figure 2.10 Model of 3x3 RVE-s under vertical axial load.

Following constraints on edges of RVE are obtained:

$$u(0, y) = 0$$

$$u(b, y) = \text{const} = \delta_x$$

(2.54)

$$u(x, 0) = u(x, L)$$

$$v(x, L) - v(x, 0) = \text{const} = \delta_y$$

However, in FEA it is practically difficult to couple horizontal edges in x and y directions while applying an axial load on the same edges. This is due to reason that vertical axial force distribution that causes natural deformation shape is not known *a priori*. Therefore, the vertical load case is realised by partially including the neighbouring openings of studied RVE in the model. It is sufficient to model the panel above and below the studied RVE until half height of the opening to achieve natural deformation field on the RVE. The proposed boundary conditions for submodel on Figure 2.11 are:

$$u(0, y) = 0$$

$$u(b, y) = \text{const} = \delta_x$$

(2.55)

$$v(x, -L_2) = 0$$

The horizontal axial loading is modelled by forced vertical displacement on top edge. The force F_y is obtained as interface load acting on sections $y = L$ and $y = 0$.

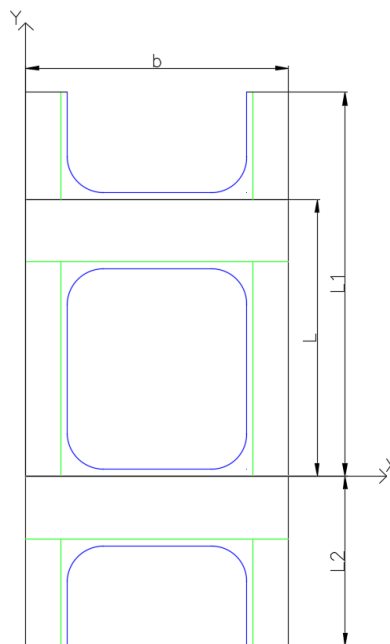


Figure 2.11 Submodel for vertical axial load case.

The axial average strain can be expressed as

$$\begin{aligned}
\bar{\varepsilon}_{yy} &= \frac{1}{2V} \int_S (u_y n_y + u_y n_y) dS = \frac{1}{V} \int_S u_y n_y dS = \\
&= \frac{1}{V} \int_L (u_{y,top} - u_{y,bottom}) t dL = [The vertical displacements of nodes at y = \\
&= 0 \text{ and } y = \\
&= L \text{ are naturally coupled due to periodicity of the structure, thus } (u_{y,top} \\
&- u_{y,bottom} = \delta_y) = \frac{1}{Lbt} t b \delta_y = \frac{\delta_y}{L},
\end{aligned} \tag{2.55}$$

where

$$v(x, L) - v(x, 0) = const = \delta_y. \tag{2.56}$$

From external work strain energy equivalence:

$$W = \frac{1}{2} F_y \delta_y = \frac{1}{2} \bar{\sigma}_{yy} \bar{\varepsilon}_{yy} V = \frac{1}{2} \bar{\sigma}_{yy} \frac{\delta_y}{L} V, \tag{2.57}$$

the average stress $\bar{\sigma}_{yy}$ is

$$\bar{\sigma}_{yy} = \frac{F_y}{bt}. \tag{2.58}$$

The equivalent properties can be obtained according to compliance matrix (2.44) from:

$$\bar{\varepsilon}_{yy} = -\frac{\nu_{xy}}{E_x} \bar{\sigma}_{xx} + \frac{1}{E_y} \bar{\sigma}_{yy} + C_{23} \bar{\sigma}_{xy}, \tag{2.59}$$

$$\bar{\varepsilon}_{xy} = C_{31} \bar{\sigma}_{xx} + C_{32} \bar{\sigma}_{yy} + \frac{1}{2G_{xy}} \bar{\sigma}_{xy}. \tag{2.60}$$

According to analysis $\bar{\sigma}_{xx} = \bar{\sigma}_{xy} = 0$ and $\bar{\varepsilon}_{xy} = 0$, therefore

$$\bar{\varepsilon}_{yy} = \frac{1}{E_y} \bar{\sigma}_{yy} \Rightarrow E_y = \frac{\bar{\sigma}_{yy}}{\bar{\varepsilon}_{yy}} = \frac{F_y L}{\delta_y b t}, \tag{2.61}$$

$$\bar{\varepsilon}_{xy} = C_{32} \bar{\sigma}_{yy} \Rightarrow C_{32} = \frac{\bar{\varepsilon}_{xy}}{\bar{\sigma}_{yy}} = 0. \tag{2.62}$$

Thus, there is no coupling between axial and shear terms.

SHEAR EQUIVALENCE

The boundary conditions for RVE with offset opening and stiffeners under in plane shear loading are established by analysing a structure of 3x3 RVE-s, Figure 2.12. The natural displacement field and boundary conditions are obtained from central RVE as it is sufficiently removed from boundaries.

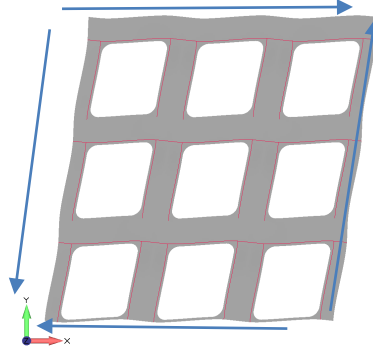


Figure 2.12 Model of 3x3 RVE-s under shear load.

Following boundary conditions are proposed for single RVE, Figure 2.13:

$$u(0, y) = u(b, y)$$

$$v(0, y) = v(b, y)$$

(2.63)

$$u(x, L) - u(x, 0) = const = 2\delta_x$$

$$v(x, 0) = v(x, L)$$

Additionally, vertical boundaries are constrained to constant lateral displacement as for RVE with central opening which was determined to be natural deformation shape from analysis of structure of 3x3 RVE-s.

$$\varepsilon_{yy}(0, y) = \varepsilon_{yy}(b, y) = 0 \text{ or } v(0, y) = v(b, y) = \delta_y \quad (2.64)$$

Horizontal edges however cannot be constrained for constant lateral displacement as in case of RVE with central opening as symmetry is violated with respect to horizontal axis.

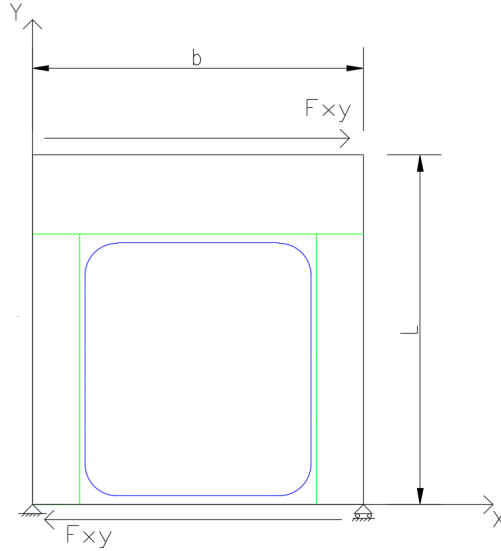


Figure 2.13 RVE with offset opening and stiffeners for shear load case.

For shear load case, equal and opposite shear loads F_{xy} are applied on edges $y = 0$ and $y = L$. The RVE is pinned at $(0; 0)$ and on roller at $(b; 0)$ to eliminate rigid body motion ($\delta_y = 0$). The pin and roller constraint reactions at bottom corners result in shear load on vertical sides of the model. Therefore, the RVE is loaded with pure shear. Average in plane shear strain is obtained from

$$\bar{\gamma}_{xy} = \frac{2}{V} \int_V \varepsilon_{xy} dV = \frac{1}{V} \int_S (u_x n_y + u_y n_x) dS = \frac{1}{V} \int_S (u_x n_y) dS = \frac{2\delta_x}{L}. \quad (2.65)$$

Form external work-strain energy equilibrium

$$\frac{1}{2} F_{xy} 2\delta_x = \frac{1}{2} \bar{\sigma}_{xy} \bar{\gamma}_{xy} V \quad (2.66)$$

$$= \bar{\sigma}_{xy} \delta_x bt,$$

$$\bar{\sigma}_{xy} = \frac{F_{xy}}{bt}. \quad (2.67)$$

The effective in plane shear modulus is found as

$$G_{xy} = \frac{\bar{\sigma}_{xy}}{\bar{\gamma}_{xy}} = \frac{F_{xy} L}{bt 2\delta_x}, \quad (2.68)$$

Where $2\delta_x$ is horizontal displacement of edge $y = L$ relative to edge $y = 0$.

2.4 Limitations in equivalent orthotropic modeling

2.4.1 Equivalency in forces and moments

The homogenization of RVE is based on strain energy equivalence according to average stresses and strains. The use of classical theory is valid for application to panels with central opening for which stress distributions for uniaxial load cases on the edges of RVE are symmetric and equivalence in forces (eq. 2.69) and moments (eq. 2.70) between heterogeneous and homogenized media are achieved as shown on Figure 2.14.

$$\frac{F_x}{2} + \frac{F_x}{2} = \int_0^L \sigma_{xx} t dy \quad (2.69)$$

and

$$M_z \left(y = \frac{L}{2} \right) = \int_0^L \sigma_{xx} t y dy = -\frac{L}{2} \frac{F_x}{2} + \frac{L}{2} \frac{F_x}{2} = 0 \quad (2.70)$$

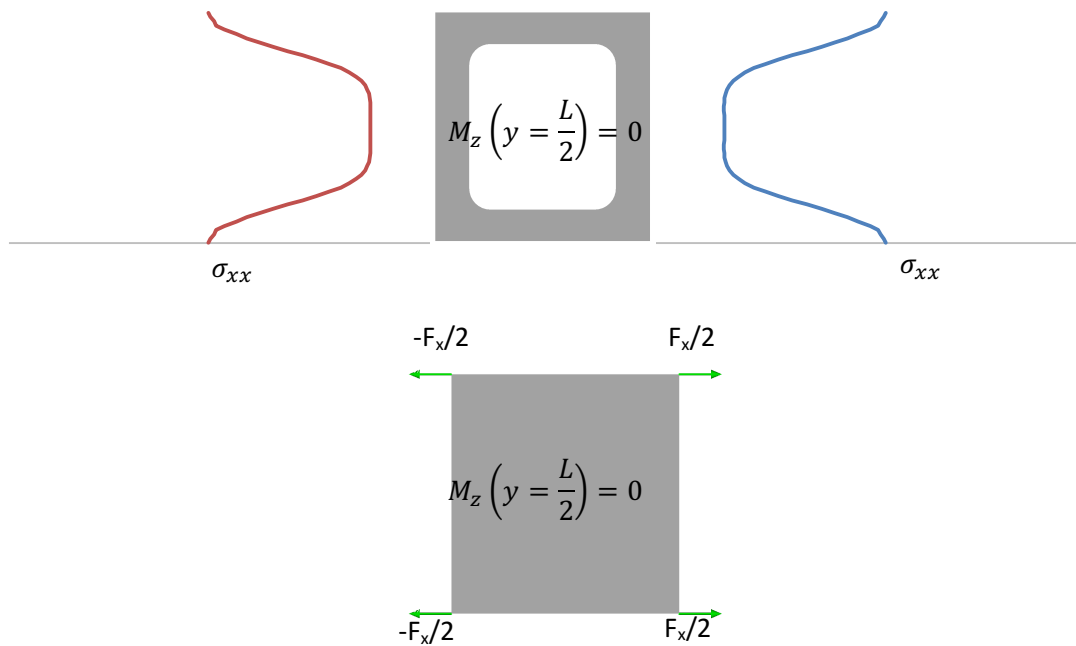


Figure 2.14 Force and moment on RVE with central opening under horizontal tension (heterogeneous explicit model - top, Homogeneous equivalent model - bottom).

In case of offset opening the stress distribution on edges of unit cell under horizontal axial load case is not however symmetric, which reveals micropolar effect [23]. This results in net moment acting on midpoint of side of heterogeneous structure as illustrated on Figure 2.15 for horizontal axial tension, while homogenized model shows no net moment about midpoint of vertical side. As result of homogenization according to classical theory the equivalency in forces (eq. 2.69) is achieved as in case of central opening. The equivalency in moments about midpoint of vertical side (eq. 2.71) is not realized.

$$M_z \left(y = \frac{L}{2} \right) = \int_0^L \sigma_{xx} t y dy \neq -\frac{L}{2} \frac{F_x}{2} + \frac{L}{2} \frac{F_x}{2} = 0 \quad (2.71)$$

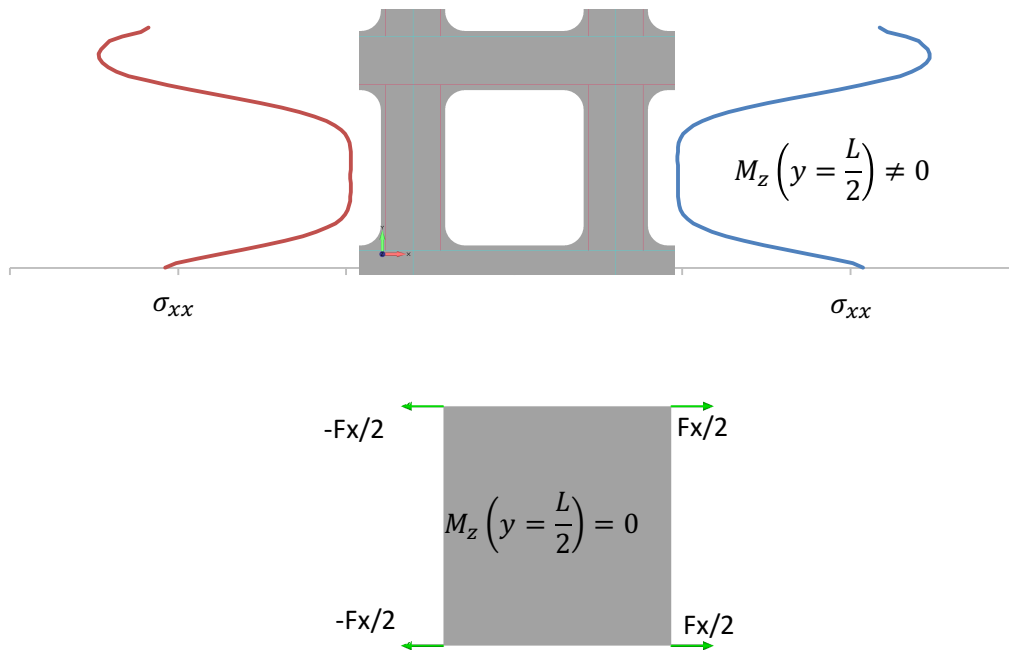


Figure 2.15 Force and moment on RVE with offset opening under horizontal tension (heterogeneous explicit model - top, Homogeneous equivalent model - bottom).

This problem can be tackled by application of couple-stress theory. In this generalization of classical elasticity for in plane problem, the stress becomes asymmetric with four components $(\sigma_{xx}, \sigma_{yy}, \tau_{xy}, \tau_{yx})$ and couple-stress (moment per unit area m_{xz}, m_{yz}) is introduced. In addition to classical strain components $\varepsilon_{xx}, \varepsilon_{yy}$ and γ_{xy} there are also curvature components κ_{xz} and κ_{yz} produced by couple-stress. Rectangular components of stress and couple-stress are presented on Figure 2.16 [24]. This generalization of classical elasticity is not implemented into commercial FEA packages and is therefore not applied in scope of this work and elements based on classical

theory of elasticity are used. The errors arising due to lack of equivalency in moments are discussed in chapter 4.

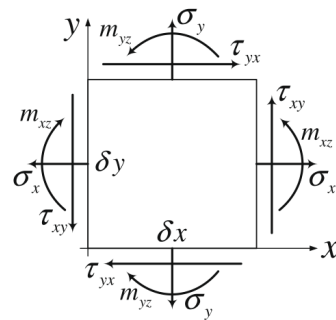


Figure 2.16 Rectangular components of stress and couple-stress [24].

2.4.2 Periodicity of structure and load

In equivalent orthotropic modeling applied to materials science the boundary layer on which the load is applied and periodicity is violated is very small compared to extent of the body [17]. In application to ship structures however the boundary layer is significant part of the homogenized structure as illustrated on Figure 2.17. Due to significant extent of boundary layer in ship structures, compromised response is expected in large part of the structure.

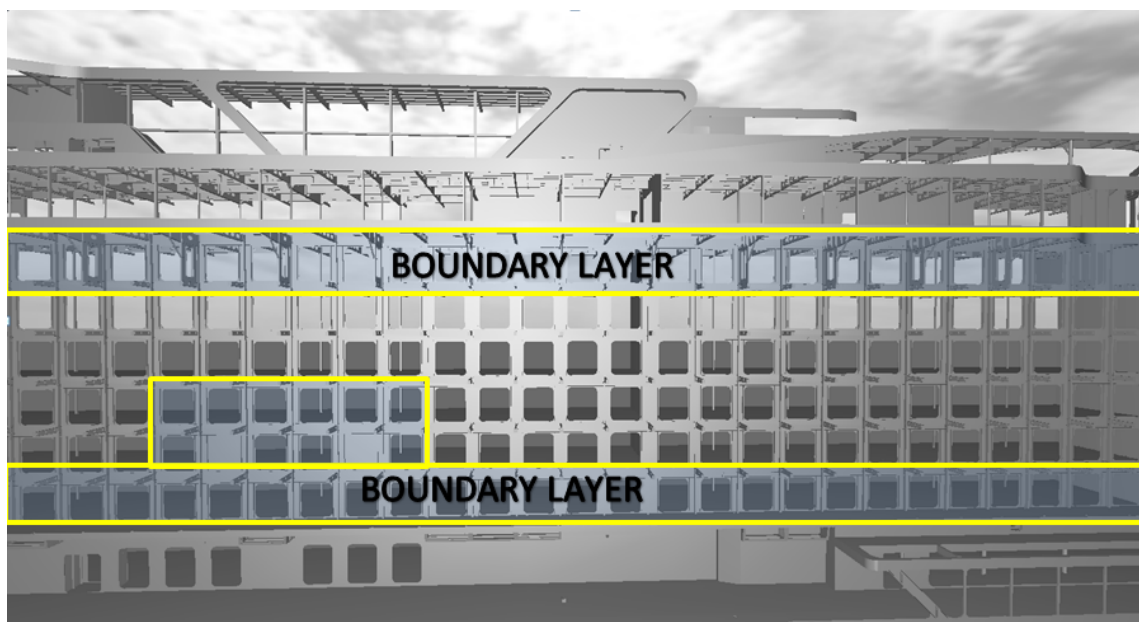


Figure 2.17 Boundary layer on ships side shell.

In addition to violation of structural periodicity, the structure is not only loaded at the boundaries of periodic grid but considerable local loads occur in side shell where adjacent longitudinal bulkheads are discontinuous. This results in significantly non-periodic stress state and large strain gradients in periodic side shell. However, periodic stress and strain field was assumed in finding boundary conditions for sub-model used for derivation of equivalent properties. Therefore, the equivalent properties are based on certain deformation shape that realizes if stress and strain fields are periodic – loading is uniform. If external load is applied on RVE in periodic structure the stress and strain fields will no longer be periodic and assumed deformation shape will not realize. Due to different deformation mode, the effective shear moduli of these unit cells will be different. The problem is illustrated on Figure 28 by two unit cells subject to 1F shear load and 3F shear load as a result of external loading in periodic grid both deforming anti-symmetrically. As seen, the deformation shapes of adjacent edges do not match. Therefore, these deformation shapes cannot realize for adjacent openings in explicit structure and actual deformation shape will differ resulting in different effective moduli. In homogenization theory, it is known as violating principle of separation of scales which assumes, that microscopic scale (unit cell) is much smaller than characteristic length over which macroscopic loading varies in global model [19]. The effect of large strain gradients is investigated in chapter 4.4.2 by comparison of box-like ship response with continuous and discontinuous longitudinal bulkheads. The influence of boundary layer to global response is evaluated in chapter 4.4.1.

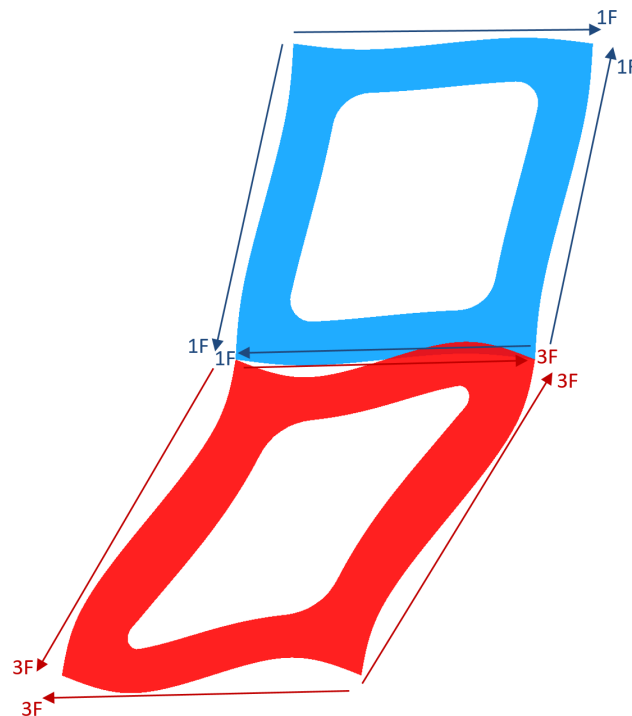


Figure 2.18 Antisymmetric deformation of unit cells under pure shear load (1F - top and 3F - bottom).

2.5 Inclusion of stiffeners and window frames in equivalent modelling

Since in case of equivalent orthotropic modeling a plate with a cutout is replaced by single or few equivalent shell elements the stiffeners, window frames and insert plates cannot be modeled explicitly due to incompatibility with coarse equivalent mesh. The contribution of stiffeners and window frames to equivalent shear modulus has been neglected in past research [6], [18], [22], [25] with exception of Fransman [5], who included window frame's contribution in equivalent shear modulus derivation.

In case of typical balcony openings there are vertical stiffeners close to vertical sides of opening and single longitudinal stiffener above the opening. The vertical stiffeners have major contribution to bending stiffness of vertical plate strips where they act as flanges for vertical plate strips. Horizontal stiffeners contribute similarly to bending stiffness of horizontal plate strips. In addition to contribution to bending stiffness of the plate strips, both vertical and horizontal stiffeners carry shear loads when shear deformation of plate strips is considered. The contribution of stiffeners to effective shear modulus of single opening is presented in chapter 4.1.

3. DIRECT MODELING OF OPENINGS WITH COARSE MESH

The global model of ship is composed of coarse mesh as shown on Figure 3.1. The areas such as window and balcony openings in the side shell are modelled with simplified geometry and coarse mesh. As a result, accuracy of response depends on mesh size which was studied for centrally placed rectangular window by Fricke [25], but also on simplification of structure for compatibility with coarse mesh size. Later involves excluding corner radius and insert plates, lumping of stiffeners and offsetting the opening. These factors have moderate effect on axial stiffness properties but significant effect on shear stiffness of an opening. In following the effect of simplification only to shear stiffness is discussed.

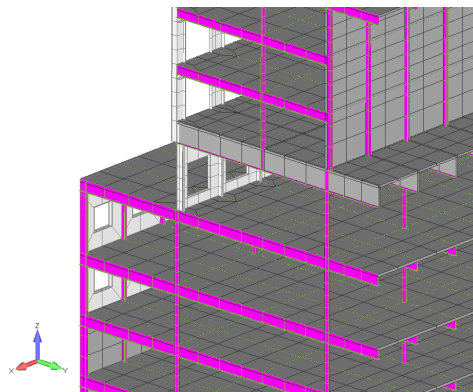


Figure 3.1 Section of global coarse mesh model.

3.1 Effect of simplification of structure to shear stiffness

In order to understand, how stiffeners and window frames contribute to in plane shear stiffness of panel with cutout, it is necessary to look at the components contributing to shear stiffness as illustrated on Figure 3.2:

1. Undeformed opening
2. Shear deformation of vertical and horizontal plate strips
3. Local deformation at intersection plate of vertical and horizontal plate strips
4. Bending of vertical plate strips
5. Bending of horizontal plate strips

Shear deformation components 2 and 3 are present in all types of opening. The bending components 4 and 5 are less pronounced for small openings with wide and short plate strips and more pronounced for large balcony openings with long narrow plate strips between openings. For accurate response, all components need to be accurately accounted.

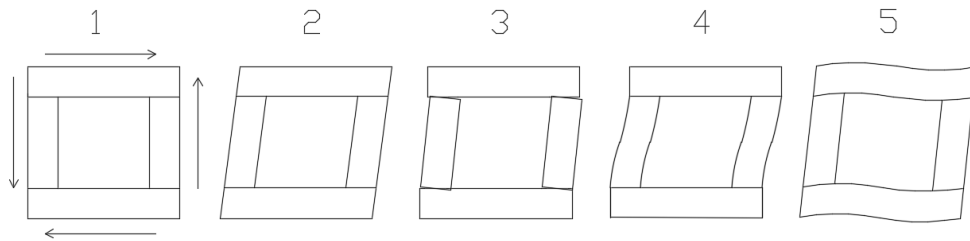


Figure 3.2 Shear deformation components of an opening.

The proposed simplification to balcony openings for coarse mesh modeling includes neglecting corner radius (Figure 3.3, b), offsetting the opening to bottom of the panel and lumping stiffeners to side of the opening (Figure 3.3, c). First is necessary as rounded corners cannot be included in coarse mesh. Later is needed to avoid using elements with very high aspect ratio to model bottom plate strip of the panel. The stiffeners are lumped to sides of the opening to comply with coarse mesh. Height L_0 and width b_0 of the opening remains constant while corner radius is excluded.

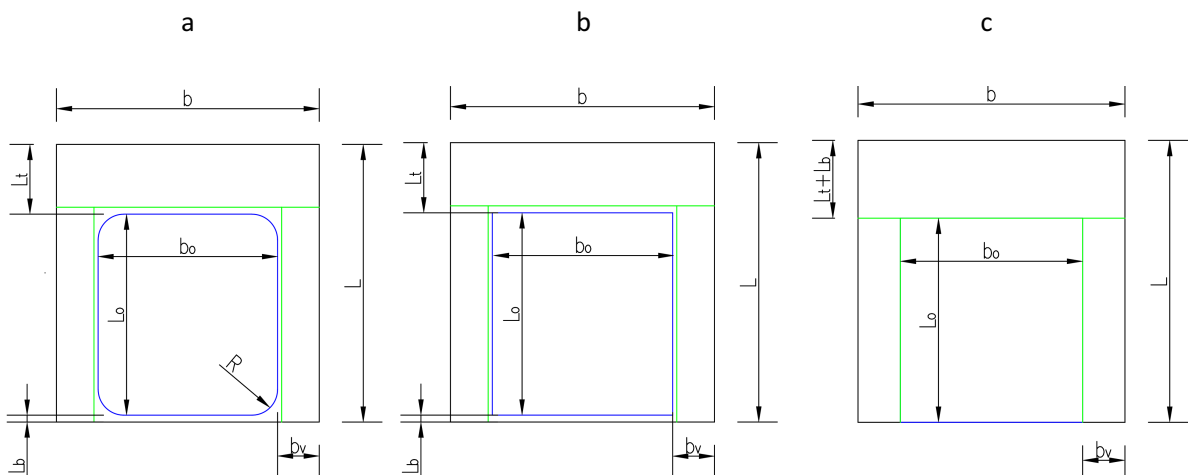


Figure 3.3 Simplification of balcony opening for coarse mesh modelling. a – explicit model, b – neglecting of corner radius, c – offsetting the opening to bottom of the panel and lumping stiffeners to side of the opening.

Neglecting corner radius has major effect on bending of vertical and horizontal plate strips at intersection of vertical and horizontal plate strips due to locally reduced section modulus in

simplified model as illustrated on Figure 3.4. In explicit model, the section modulus of vertical plate strips is $I(R, y) = \frac{(b_v + f(R, y))^3 t}{12}$, while in simplified model section modulus is constant $I = \frac{b_v^3 t}{12}$. As section modulus depends on third power of plate strip width, exclusion of corner radius has large influence to bending contribution to shear stiffness.

In addition, local rotation at intersection plate is larger in case of simplified model as the moment from plate strips is carried to smaller section.

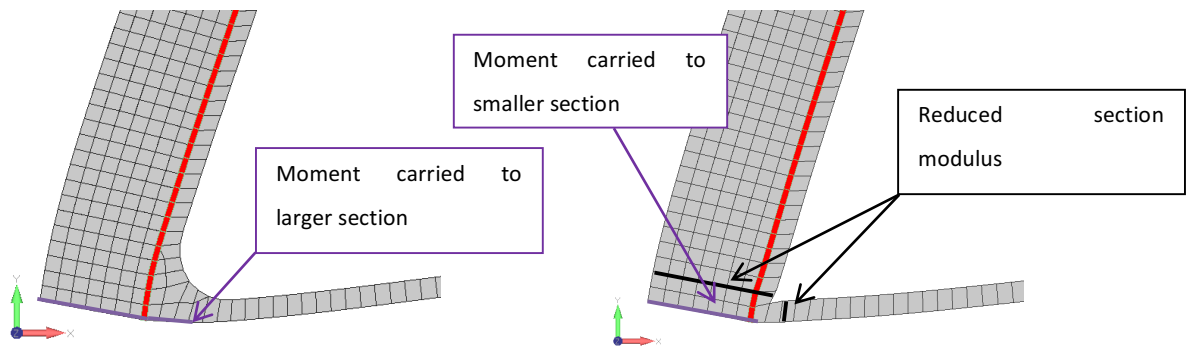


Figure 3.4 Local bending of vertical and horizontal plate strips under shear load. Explicit geometry - left, simplified model - right.

Offsetting the opening does not have major influence to shear stiffness as top and bottom edges' vertical and horizontal displacements are coupled when under shear load in periodic grid. This results in top and bottom plate strips acting as a single beam with height $L_b + L_t$ and moment of inertia $I = \frac{(L_b + L_t)^3 t}{12}$ which is equal to moment of inertia of top plate strip in simplified model, Figure 3.3 (c). The influence to shear stiffness when offsetting the opening was determined to be zero by FEA of opening constrained anti-symmetrically as in periodic grid under shear load. In case the opening is not in periodic grid, offsetting results in changed bending stiffness of bottom and top plate strips as top and bottom edge displacements are not coupled. If the offset distance would be significant relative to opening geometry, modelling by explicit geometry (no offsetting) should be considered to avoid errors due to inaccurate bending stiffness of bottom and top plate strips.

Lumping of stiffeners increases the bending stiffness of vertical and horizontal plate strips as stiffeners which act as flanges of the plate strips are moved further away from the neutral axis. This results in increased section modulus of vertical and horizontal plate strips with stiffeners.

3.2 Effect of coarse mesh size to shear stiffness

In case of 4-noded CQUAD4 plate elements and coarse mesh, the elements are not capable of accurately representing bending behavior of plate strips due to linear shape functions and parasitic shear phenomenon. CQUAD8 elements have parabolic shape functions and no parasitic shear effect but require relatively large number of nodes for modeling which would increase local mesh density and modeling effort. In addition, the mid-side nodes need to be in center 1/3 of element edge. Therefore, the sensitivity analysis for coarse mesh is only performed for CQUAD4 elements.

Since the bending is most pronounced close to intersection plate, mesh size at intersection of vertical and horizontal plate strips should be sufficiently fine to capture accurate response. Nevertheless, this kind of mesh size is too fine for practical modeling. Therefore, sensitivity analysis needs to be performed. A balance in error due to simplification of model and coarse mesh size is sought for in order to obtain modeling approach with reasonably accurate stiffness. The shear stiffness sensitivity analysis for coarse mesh is presented in 4.2.3 along with cumulative error due to simplification and mesh size.

4. RESULTS

In this chapter, the equivalent orthotropic properties are presented for central and stiffened offset balcony openings according to methods proposed in chapter 2.3. The accuracy of openings modeled with coarse mesh accounting for different mesh size and simplification of structure is presented. To evaluate the accuracy of proposed modeling techniques, two cases studies are performed. In first case, the accuracy of side shell behavior is studied to validate the modeling techniques in simple case where the side shell is loaded at its boundaries. In second case study, modeling techniques are evaluated in periodic grid and its boundaries when the loading is no longer only applied on sides of the grid but follows load carrying mechanism of a box-like ship under 4-point bending. The aim is to test the performance of modeling techniques in periodic grid and at boundary of periodic grid. In addition, the effect of significantly non-uniform loading resulting in high strain gradients is evaluated to study performance of openings in periodic grid.

4.1 Equivalent in plane properties

Equivalent in plane properties of central opening and typical balcony (Figure 4.1) openings were calculated according to procedure proposed in chapter 2.3. The mesh size was 50 mm. Side shell plating was modeled with CQUAD4 shell elements and stiffeners with CBEAM elements. The necessity to include stiffeners in calculation of equivalent shear modulus was studied by calculating effective shear modulus for typical balcony opening with and without stiffeners.

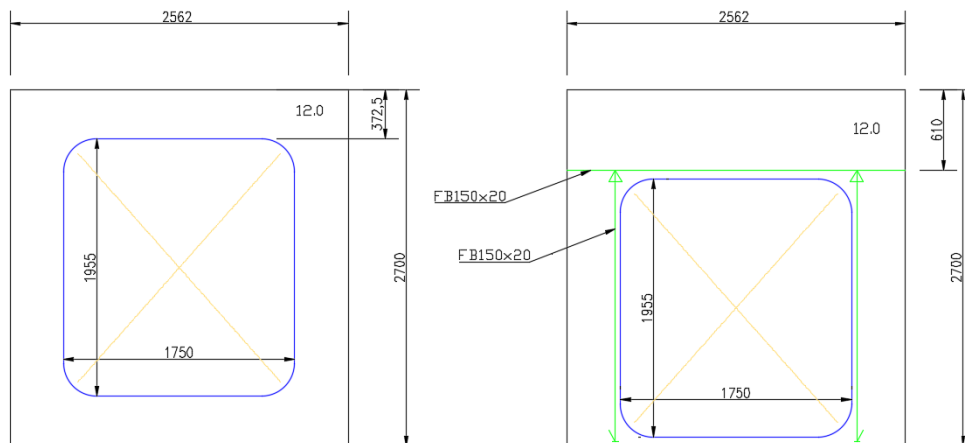


Figure 4.1 Central opening (left), typical offset balcony opening (right).

The obtained equivalent orthotropic properties are presented in Table 4.1. While the contribution of stiffeners to equivalent axial modulus is well known, its contribution to equivalent shear modulus is often neglected [6], [18], [22], [25]. It is seen that neglecting of stiffeners results in 12,3% underestimation of effective shear modulus. Therefore, inclusion of stiffeners in equivalent shear modulus calculation should not be neglected in case of large balcony openings.

Table 4.1. Equivalent orthotropic properties of balcony openings.

Description	Ex, GPa	Ey, GPa	G, GPa	ν_{xy}
Central opening	62,80	70,50	4,98	0,13
Offset opening (no stiffeners)	62,80	70,50	4,98	0,13
Offset opening (with stiffeners)	82,06	93,18	5,68	0,12

4.2 Coarse mesh modeling accuracy

The coarse mesh stiffness accuracy is determined by first studying the effect of simplification of structure and secondly due to using coarse mesh.

4.2.1 The reference model

The models against which the cost of simplification of structure and coarse mesh size is compared are presented on Figure 4.2, where the structure and geometry are same as presented on Figure 4.1. The models consist of CQUAD4 elements for side plating and CBEAM elements for stiffeners. They are constrained for out of plane displacements and rotations along deck and web-frame lines as it would be in ships side shell connected to web-frames and decks which restrict out of plate displacements. The in plane, constraints and load imposed on both reference and simplified models are same as derived for homogenization in chapter 2.3.

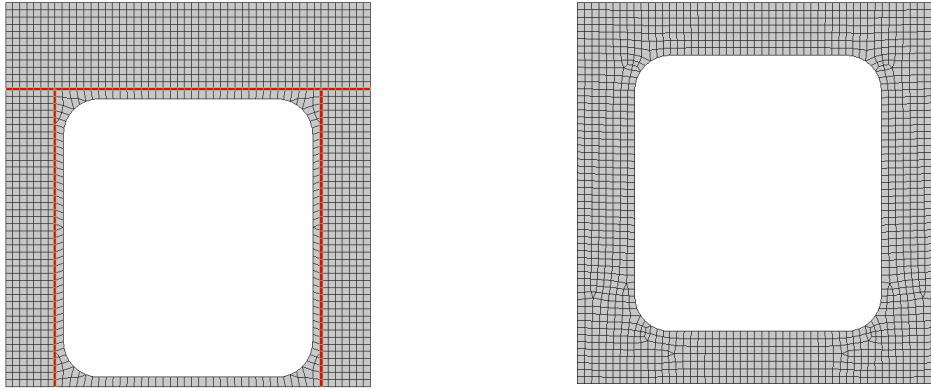


Figure 4.2 Fine mesh reference model of balcony opening. Offset – left, central – right.

4.2.2 Effect of simplification to shear stiffness

In case of modeling with coarse mesh the structure is first simplified. The effect of simplification on stiffness properties of the structure is studied by fine mesh sensitivity analysis. The effect of simplification on offset balcony opening is presented on Figure 4.3 by first excluding corner radius and then offsetting the opening to bottom of the plate while moving the stiffeners to the edge of the opening. In case of offset opening exclusion of corner radii results in 23% decrease of shear stiffness while offsetting opening and stiffeners increases shear stiffness to -17% compared to explicit value. For model with central opening only corner radius was neglected, which resulted in 26% of shear stiffness reduction.

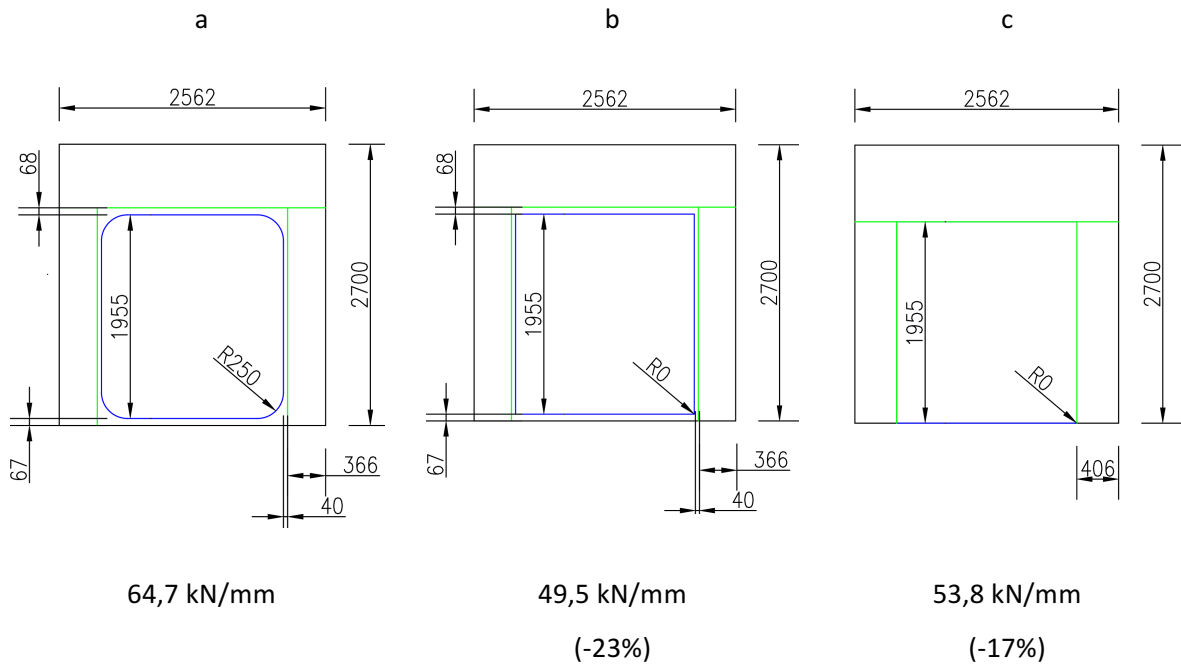


Figure 4.3 Shear stiffness due to simplification of typical balcony opening (Figure 4.1). a) explicit. b) excluded corner radii. c) excluded corner radii, opening offset to bottom edge of plate and stiffeners lumped to opening edge.

4.2.3 Effect of coarse mesh size to shear stiffness

Sensitivity analysis of mesh size to shear stiffness was performed for 4 different mesh sizes of 4x2; 4x4; 4x6 and 6x8 plate elements per panel. The results for typical balcony opening are presented in Figure 4.4. The modeling option with 8x6 elements gives 19,9 % increase of shear stiffness compared to simplified fine mesh model, accounting for error due to simplification of geometry, the total stiffness error becomes -0,2%. In case of 4x6 elements the cumulative error is 10,5% due to overestimated bending stiffness of vertical and horizontal plate strips. The cumulative error for 4x4 mesh is 12,8%, while overestimation of shear stiffness by 4x2 elements model is 41,9%. Later is assigned to fact that single elements for vertical plate strips do not allow curved bending shape to realize, with high aspect ratio being another source of error.

In case studies for offset opening coarse mesh size of 4x4 elements is applied as it is considered the best compromise between modeling effort, calculation time and stiffness accuracy. For central opening the mesh size of 4x5 elements is used for reasonable aspect ratio of vertical plate strip elements. This results in cumulative shear stiffness increase of 5,1% compared to fine mesh reference.

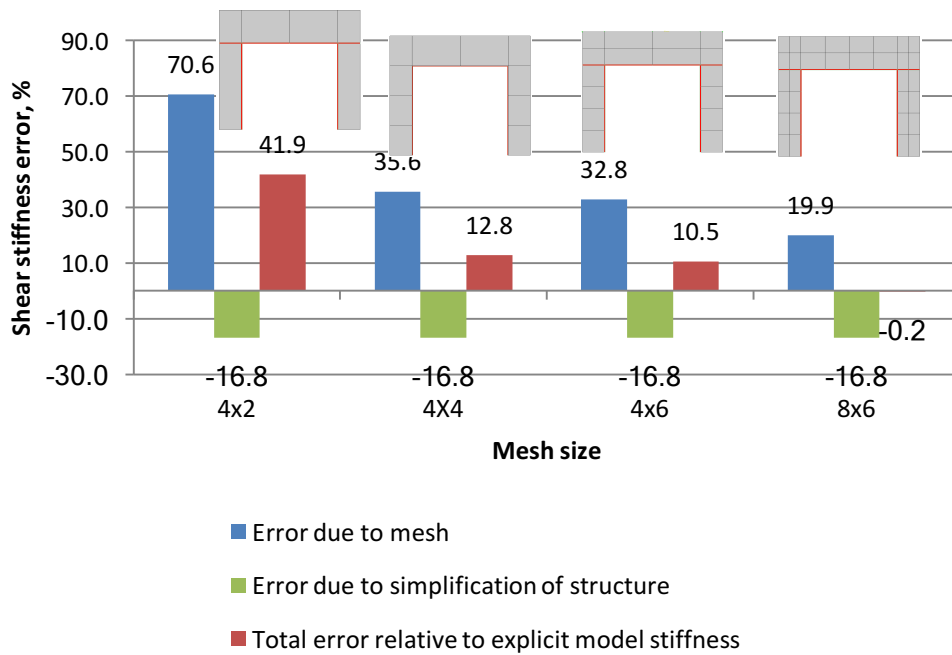


Figure 4.4 Shear stiffness modelling accuracy of typical balcony opening.

4.3 Case study 1 - Periodic side shell

In this study, the orthotropic and coarse modeling techniques are evaluated in side shell model for uniaxial and shear load cases. The periodic side shell model for offset openings is presented on Figure 4.5 and consists of CQUAD4 shell elements for side shell plate and CBEAM beam elements for stiffeners. The structure of single opening is same as presented on Figure 4.1. The model represents a periodic part of side shell.

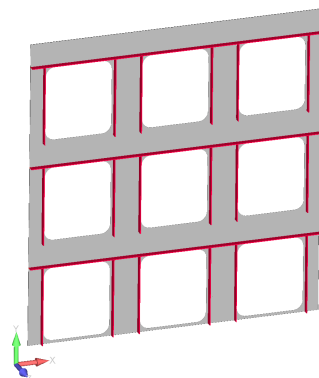


Figure 4.5 Periodic side shell test model.

4.3.1 Axial response

The structure is constrained and loaded as shown on Figure 4.6. The horizontal and vertical axial response are compared in terms of axial force required to cause 1 mm horizontal or 1 mm vertical displacement of loaded edges respectively. The orthotropic model shows accurate response for horizontal load case and 2,2% smaller stiffness compared to reference for vertical tension load case as shown in Table 4.2. The difference in case of vertical tension originates from edge effect – the horizontal edges of the model are forced straight, while equivalent elements were derived assuming periodic boundary conditions. For coarse model, horizontal axial stiffness is overestimated by 1,7% and vertical axial stiffness by 2,5%. In either case the accuracy is considered sufficient.

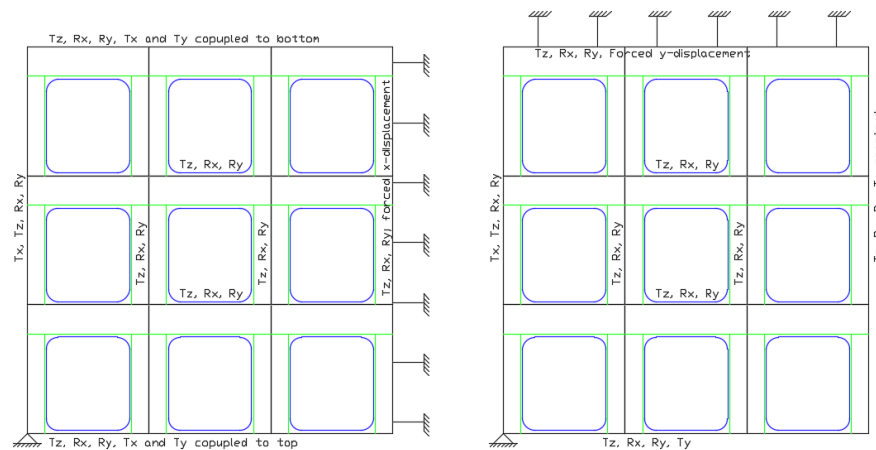


Figure 4.6 Submodel of 3x3 openings in side shell constrained and loaded for horizontal tension load case (left) and vertical tension load case (right).

Table 4.2. Axial forces causing 1 mm displacement of vertical/horizontal side of side shell model.

Model	F_x , kN	F_y , kN	Error F_x , %	Error F_y , %
Fine	1038,0	1085,2		
Orthotropic	1037,9	1061,2	0,0	-2,2
Coarse	1036,1	1112,0	1,7	+2,5

4.3.2 Shear response

For evaluation of shear response, the structure is constrained as shown on Figure 4.7: out of plane displacement and rotations are constrained along deck and web-frame lines, top and bottom

edges are coupled in x and y direction by constraint equations. Vertical edges of the model are constrained to zero vertical strain which was determined to be natural deformation shape under pure shear loading, see chapter 2.3.3. Bottom corners are placed on roller and pin. Vertical reaction force of the roller and pin act as shear force on vertical sides of the model as shown on Figure 4.8. Evaluation of shear stiffness accuracy is based on horizontal displacements along web frame lines. The horizontal displacement curves are presented on Figure 4.8. For uniform loading the orthotropic model shows accurate results at corner nodes of RVE-s, while the coarse model shows 12,4% higher shear stiffness, which was predicted in chapter 4.2.3 Effect of coarse mesh size to shear stiffness.

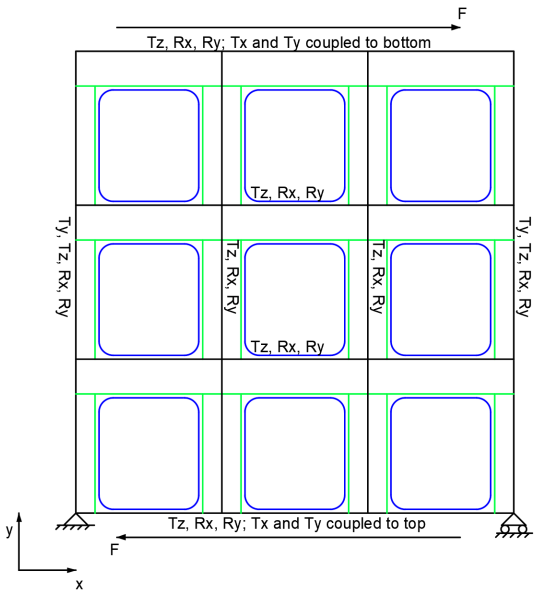


Figure 4.7 Submodel of 3x3 openings in side shell constrained and loaded for shear load case.

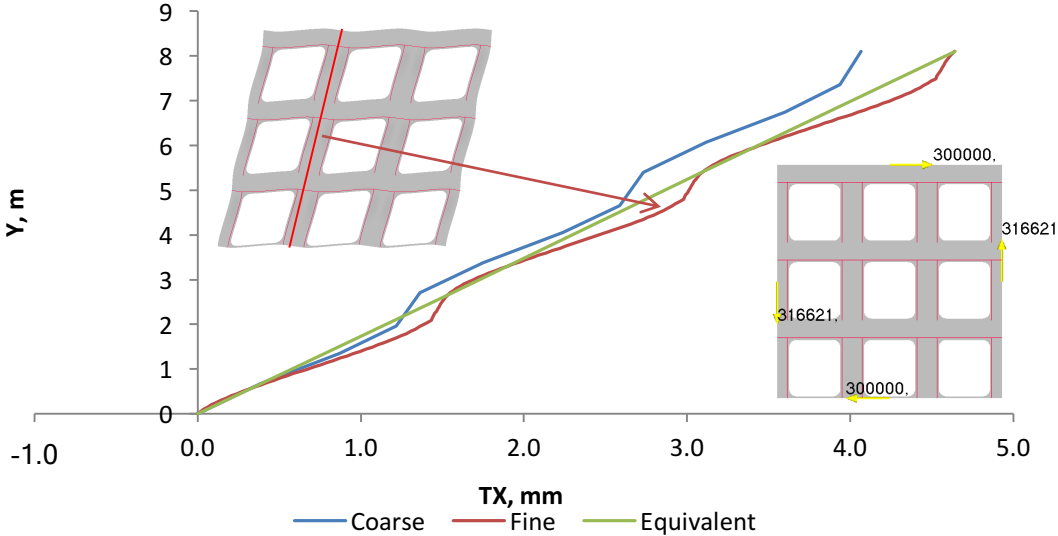


Figure 4.8 Horizontal displacement curves along web frames under shear load.

4.4 Case study 2 - Box ship with periodic side shell (4-point bending) for evaluation of periodic side shell performance

The aim of 4-point bending study for box ship is to evaluate

- performance of modeling techniques in periodic grid
- performance of modeling techniques at the edge of periodic grid
- performance of modeling techniques when loading is significantly non-uniform (large strain gradients are present)

Two box-like ship models are used. The first model (M1) is presented on Figure 4.9 and consists of decks, pillars, web frames and side shell with balcony openings. The structural scantlings are shown in APPENDIX 1. SCANTLINGS OF BOX-LIKE SHIP. As there are no internal longitudinal bulkheads the global bending and shear response is largely governed by side shell shear stiffness. The aim of the model is to evaluate performance of modeling techniques in periodic grid and at boundaries of grid. The comparison is performed based on hull girder deflection and longitudinal deck forces in bending area.

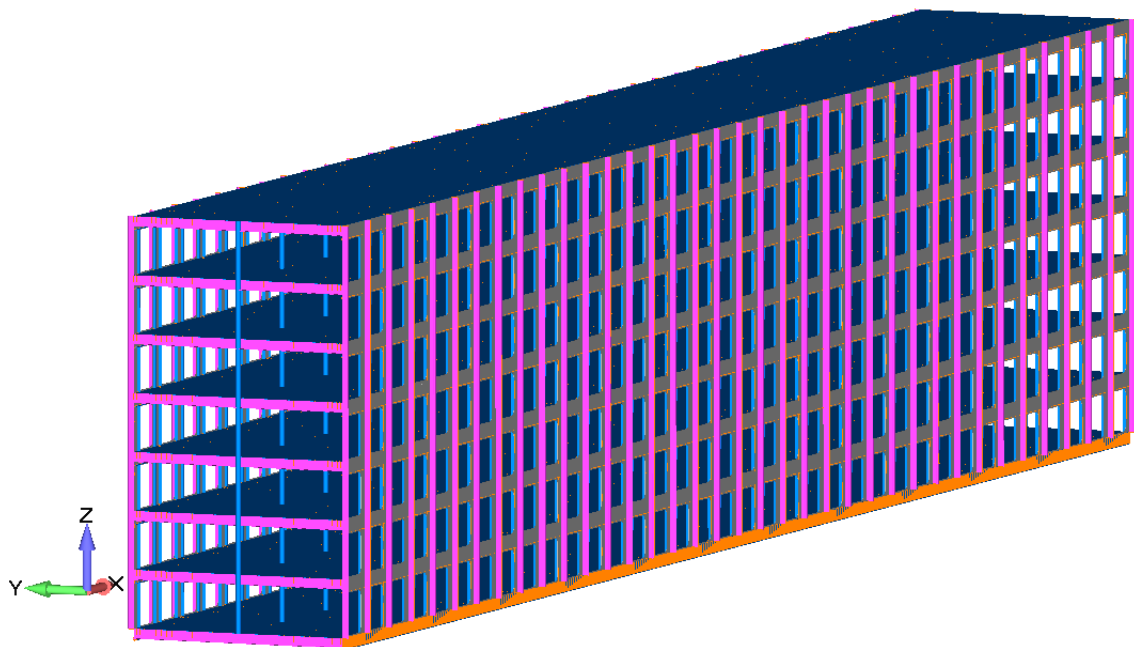


Figure 4.9 Box ship model 1 (M1).

The second model (M2) of box ship is shown on Figure 4.10. M2 is composed of longitudinal bulkhead, side shell with periodic openings, decks and web frames. The structural scantlings are shown in APPENDIX 1. SCANTLINGS OF BOX-LIKE SHIP. M2 is used for evaluation of side shell

shear forces when longitudinal bulkhead is present. Modified model M2 where discontinuous longitudinal bulkhead causes significantly non-uniform loading in side shell is used to evaluate performance of modeling techniques when large strain gradients are present. Modified model M2's structural scantlings are presented in APPENDIX 1. SCANTLINGS OF BOX-LIKE SHIP.

Both models are constrained and loaded as shown on Figure 4.11. The loads and constraints are applied to rigid elements at sections $x=0$, $x=1/3L$, $x=2/3L$ and $x=L$. The rigid elements couple y , z displacements and x , z rotations of all nodes in their longitudinal coordinate imitating the behavior of transversal bulkhead while leaving x -displacement and y -rotation free, allowing sliding between deck levels. The response is evaluated by vertical shear force in side shell at shear dominated area (region 1, $x=L/6$) and by longitudinal deck force at pure bending area (region 2, $x=L/2$).

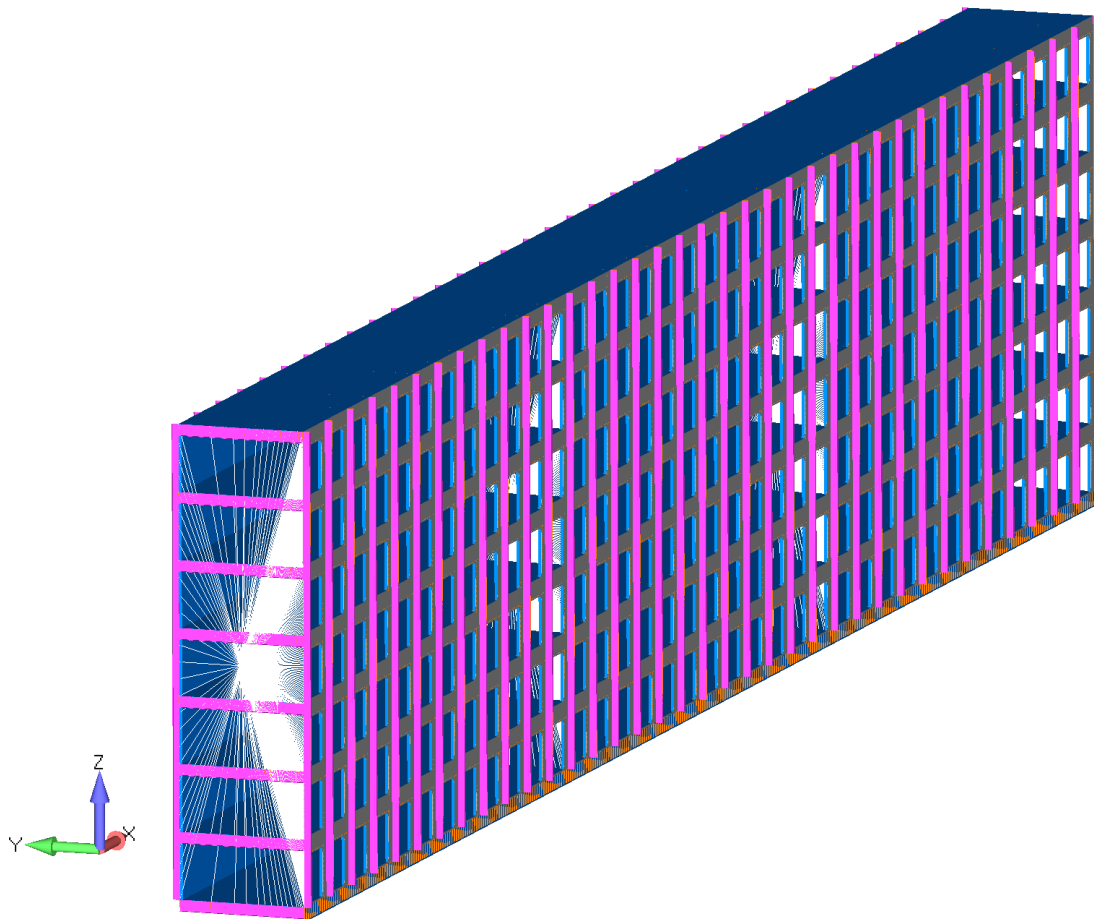


Figure 4.10 Box ship model 2 (M2).

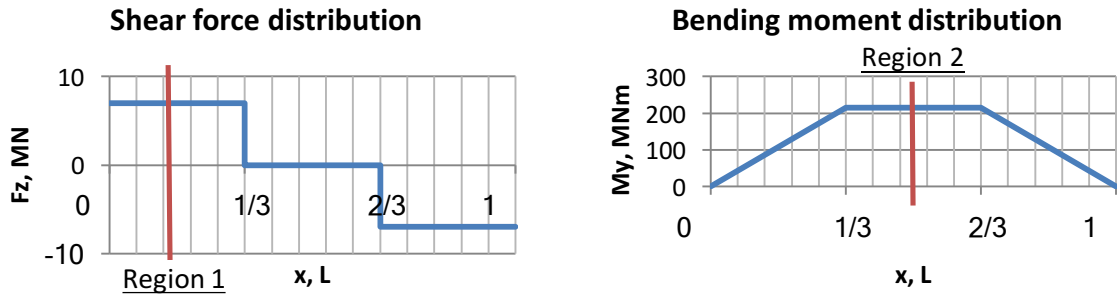
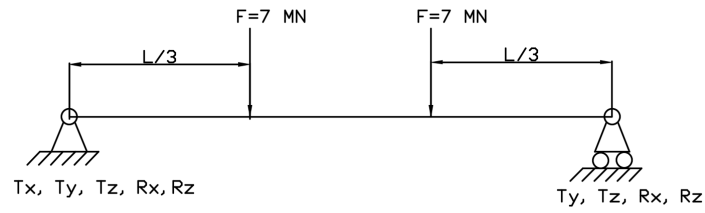


Figure 4.11 4-point bending loads.

The fine, orthotropic and coarse mesh are illustrated on Figure 4.12. In all cases the global mesh size is 2 elements per web frame spacing and 4 elements between decks. The decks and longitudinal bulkheads incorporating stiffeners are modelled with equivalent shell elements proposed by Avi [7]. Longitudinal girders, web frames and side shell stiffeners are modelled with CBEAM elements, except for side shell stiffeners in orthotropic model, which are included in equivalent orthotropic properties for side shell openings. In fine model, mesh size is locally reduced to 50 mm at side shell. The coarse model is characterized by 4 elements longitudinally and 4 (5 for model with central openings) vertically between decks and web frames at side shell. Orthotropic model was studied in 3 modifications: two CQUAD4 elements per opening (pictured), single CQUAD4 element per opening and single CQUAD8 element per opening.

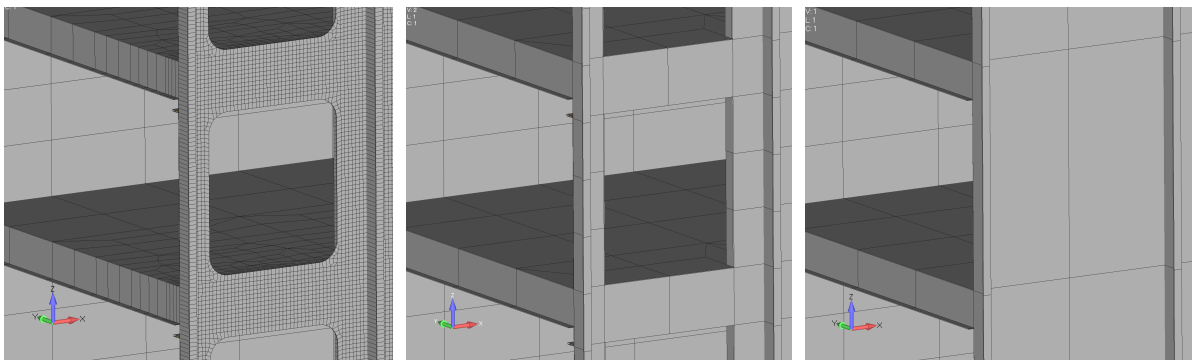


Figure 4.12 Example of fine, coarse and orthotropic mesh size for box-like ship.

4.4.1 Performance of modeling techniques in periodic grid and boundary of grid

The performance of modeling techniques in periodic grid and boundaries was evaluated for two modifications of box like ship models: openings in the center of RVE and offset openings on stiffened RVE. Firstly, the global response is evaluated based on global deflection and longitudinal deck forces in model M1 and secondly side shell modeling accuracy is evaluated by side shell shear forces in model M2.

M1 with central openings

The deflection of fine, orthotropic and coarse models are 131,1 mm, 132,3 mm and 126,5 mm respectively, orthotropic model being 1,1 % more flexible and coarse 3,4% less flexible than reference. Deflection curves along all deck lines are within 1% for each model, curves of bottom deck-side shell intersection line are presented on Figure 4.13. It is seen that there is no significant difference whether one or two 4-noded or single 8-noded element is used for orthotropic mesh, which indicates that shear locking is negligible in global model and linear shape functions and single integration point for 4-noded element is in practice not significantly less accurate than 8-noded elements. The sensitivity of side shell shear stiffness to hull girder deflection is shown by modifying orthotropic model side shell shear stiffness by $\pm 15\%$. It is seen that deflection significantly depends on orthotropic element shear stiffness while accurate result is obtained with proposed technique.

Figure 4.14 shows deflection difference of coarse and orthotropic models compared to fine mesh reference. In shear dominated area, it is seen that orthotropic model does not produce periodic deflection curve such as fine mesh model. In shear area, the coarse model shows slightly different but also periodic deflection curve, hence the rough curve. The difference in periodicity is because fine model gives accurate warping of plate strips between openings under shear load, while orthotropic model does not show any warping and coarse model does not produce accurate warping shape due to mesh size. In pure bending area, the warping of plate strips is negligible and difference between fine mesh and both alternative models is close to constant.

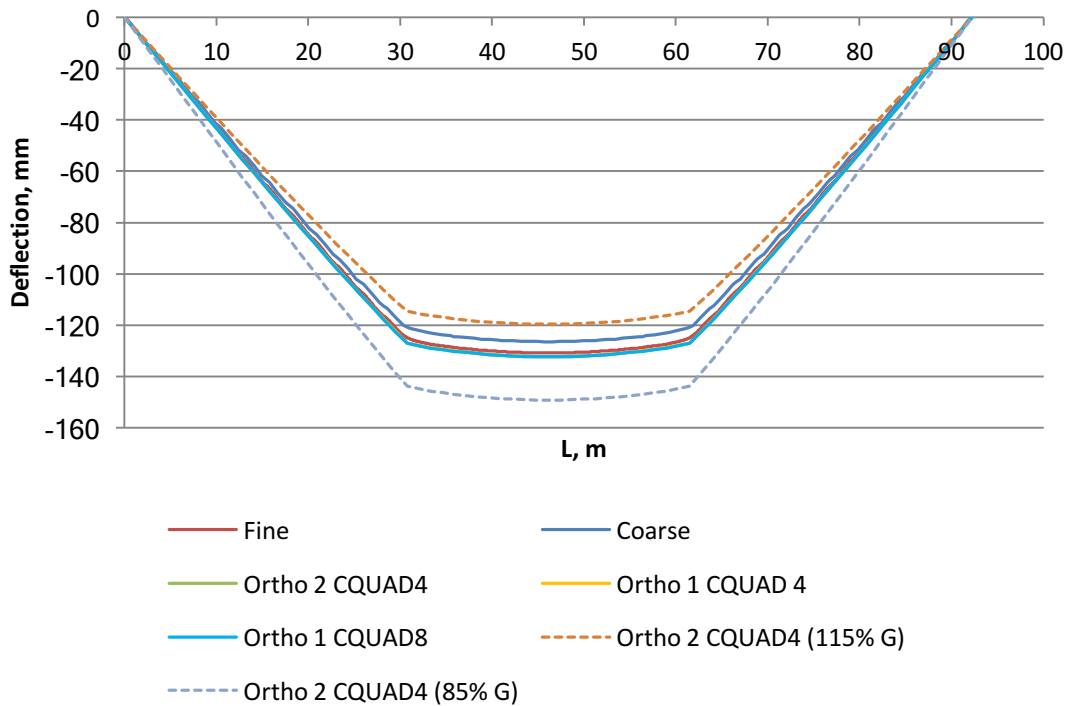


Figure 4.13 Deflection curves along deck 0 - side shell intersection line, M1 central openings.

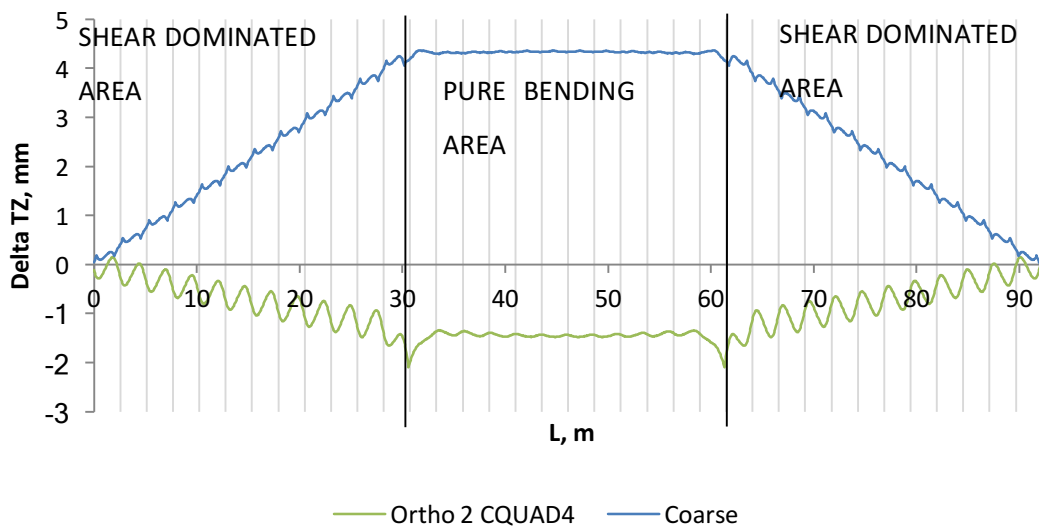


Figure 4.14. Deflection difference of coarse and orthotropic models compared to fine mesh, M1 central openings.

Longitudinal deck forces in midship area are presented on Figure 4.15. All models have similar longitudinal force distribution. From fine model curve, it is seen that the model does not behave like a beam as predicted according to Figure 1.1: top and bottom decks carry more longitudinal

force than they would in case of linear distribution. Higher deck force of orthotropic models at bottom and top decks are explained by boundary effect in orthotropic modelling. The orthotropic model overestimates the shear stiffness of top and bottom deck openings which results in 5,0% higher deck force on top deck while coarse model error is less than 0,4% at top and bottom decks.

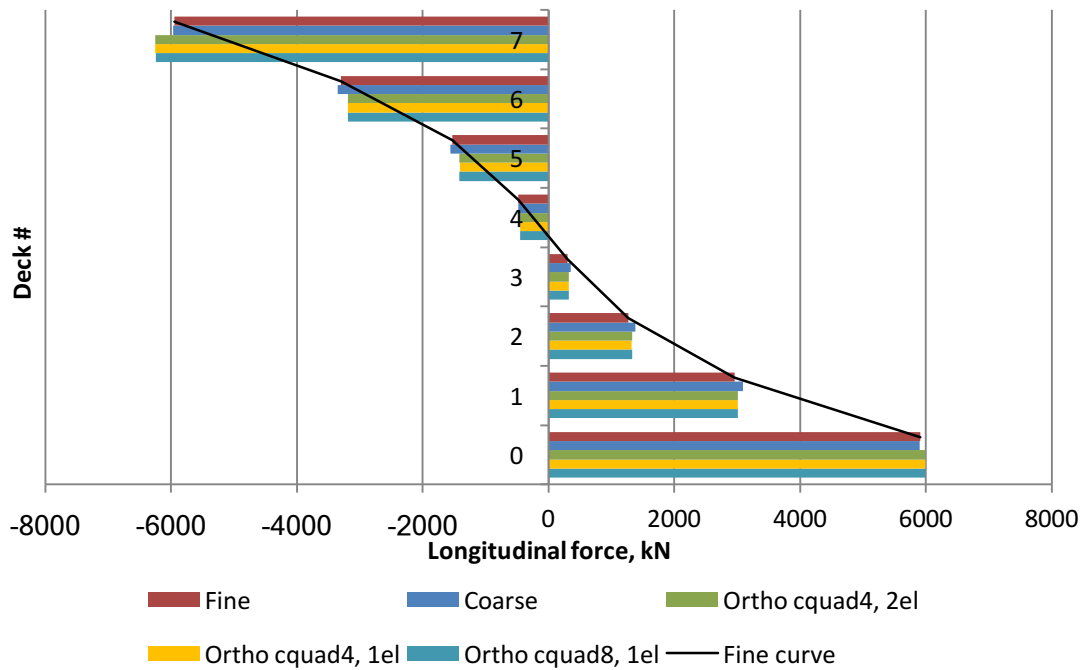


Figure 4.15 Longitudinal deck forces in region 2, M1 central openings.

M2 WITH CENTRAL OPENINGS

The accuracy of side shell modeling is evaluated based on side shell vertical shear force at region 1, Figure 4.16. Considering orthotropic model, the shear force error between decks 2-5 is under 12% and considerably higher near boundaries of periodic grid. The inaccuracy in border areas of periodic grid originates from violation of periodicity assumption. The smaller errors inside grid are result of errors in border area translating into the grid. The shear forces acting on opening at deck 6-7 in explicit fine mesh model (Figure 4.16) show that shear forces on border opening are significantly different on opposite edges which homogenized material cannot accurately describe. The shear forces acting on opposite edges of an opening at deck 3-4 area are close to being equal and the response of orthotropic model is closer to explicit behavior.

Similarly to model M1, there is no significant difference whether one or two CQUAD4 or single CQUAD8 element is used for orthotropic mesh.

For coarse mesh, the shear force error is less than 7% except for deck 0-1, where larger error is present due to parasitic shear phenomenon which occurs in 4-noded shell element next to longitudinal girder below side shell. If longitudinal girder shear forces are added to deck 0-1 then reference shear force is 35,8 kN and coarse model 26,1 kN.

Total vertical shear force through side shell is 2,3% more than reference for coarse model and 8,2% less for orthotropic model, which indicates better overall accuracy of coarse mesh model.

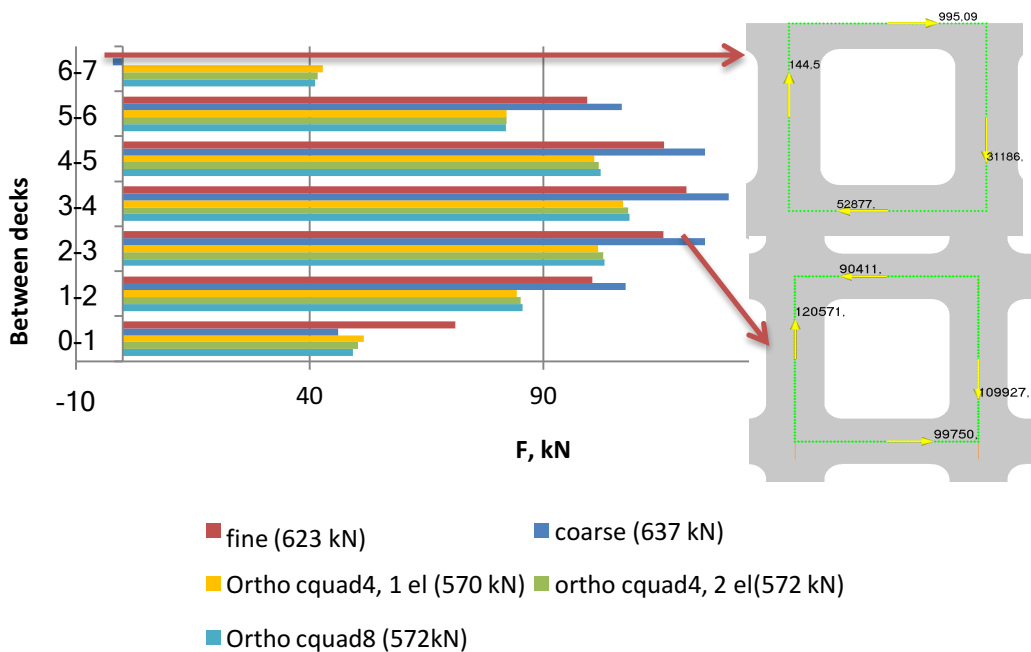


Figure 4.16 Vertical shear forces in side shell, region 1, M2 central openings.

M1 WITH OFFSET OPENINGS

The deflection of fine, orthotropic and coarse models are 117,3 mm, 118,8 mm and 118,4 mm respectively, orthotropic model being 1,3 % and coarse 0,9% more flexible than reference. Deflection curves along bottom deck – side shell intersection line are presented on Figure 4.17. Close deflection curves indicate that both modeling techniques result in sufficiently accurate global deflection when large periodic structure is considered.

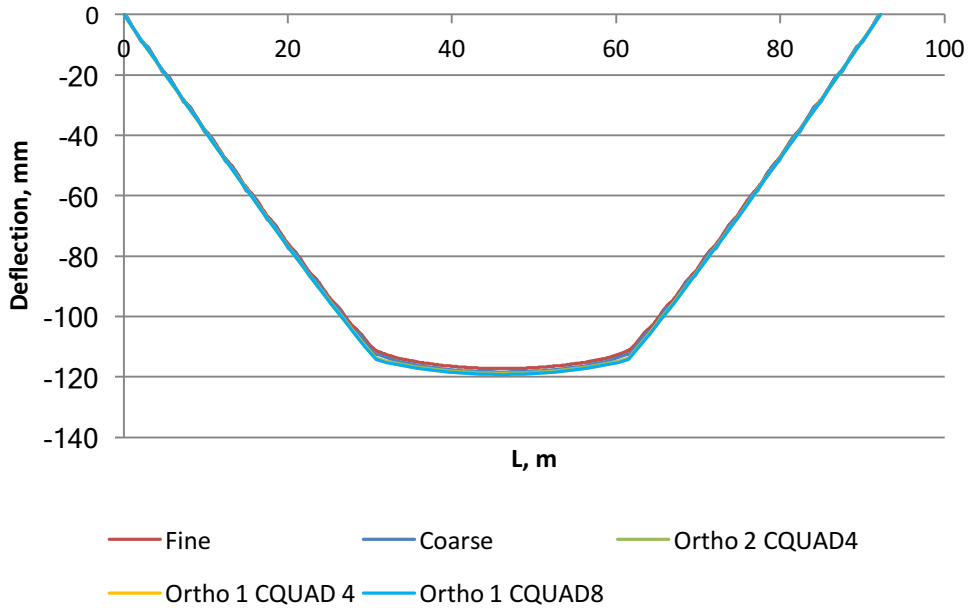


Figure 4.17 Deflection curves along deck 0 - side shell intersection line, M1 offset openings.

Longitudinal deck forces diagram on Figure 4.18 shows orthotropic model's boundary effect at top and bottom decks. As a result of higher shear stiffness of coarse model side shell the longitudinal force distribution is more beam-like than reference.

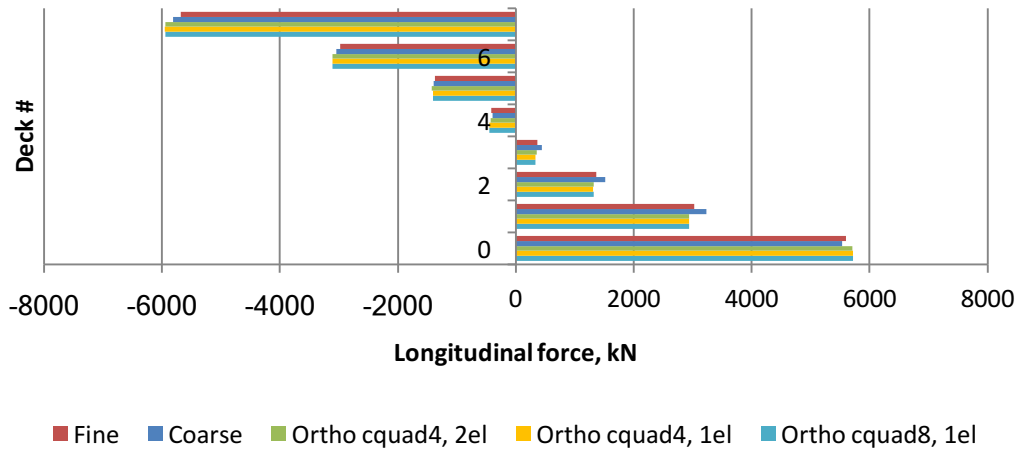


Figure 4.18 Longitudinal deck forces in region 2, M1 offset openings.

Even though micropolar effect is clearly observed due to offset openings as illustrated by moments M_y about midpoint of vertical side of openings on Figure 4.19, its effect to global response is small. The reason being that side shell contribution to longitudinal axial response is small compared to decks'.

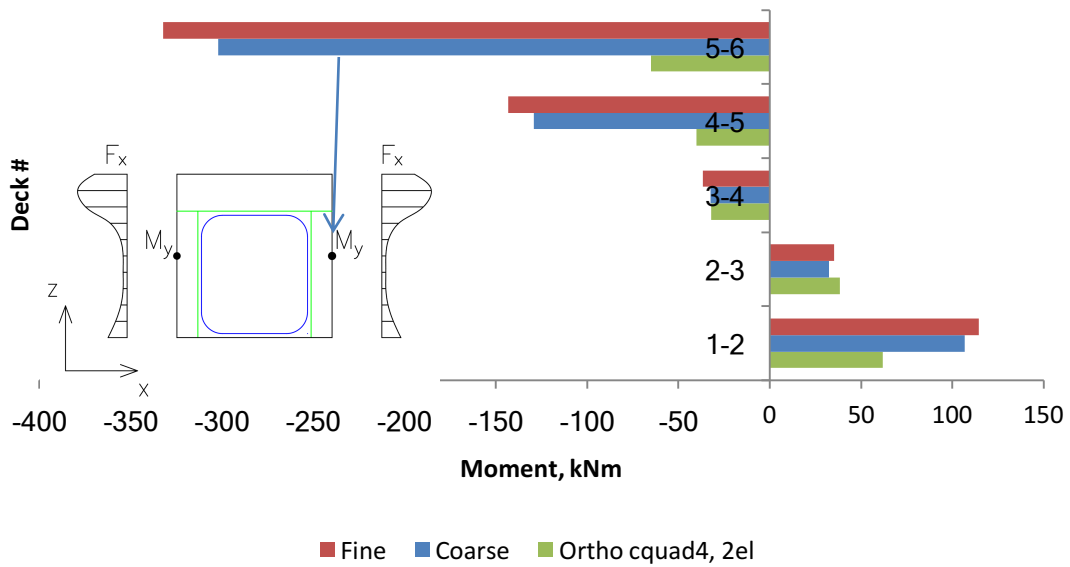


Figure 4.19 Moments M_y of in plane forces about mid-height of an opening, region 2 (mid-ship), M1 offset openings.

M2 WITH OFFSET OPENINGS

Side shell vertical shear force is presented on Figure 4.20. The orthotropic model forces show better than 17% error between decks 1-5 and significantly larger error at boundaries of the model which is assigned to violation of periodicity as in case of model with central openings.

Coarse model shows less than 5% error between decks 1-6, the error at top deck is 10% and larger inaccuracy is present at deck 0-1 which is due to same reason as in case of central openings. Additional source of error is simplification of coarse model structure by offsetting the openings to bottom of RVE and neglecting corner radius at boundary of periodic grid while coarse mesh sensitivity analysis was performed only for periodic openings.

It is also noted that for model with central openings all models showed close to parabolic shear force distribution which is normal to rectangular beam section. In this case however the idealization of parabolic shear force distribution is not valid as the openings and therefore shear center of side shell is offset in Z-direction. This is clearly seen in shear force distributions of explicit and coarse model but not evident in orthotropic model. The reason for this is that for homogeneous element the shear center is in the midpoint of the side while this is not the case for heterogeneous structure where the shear center is above the midpoint.

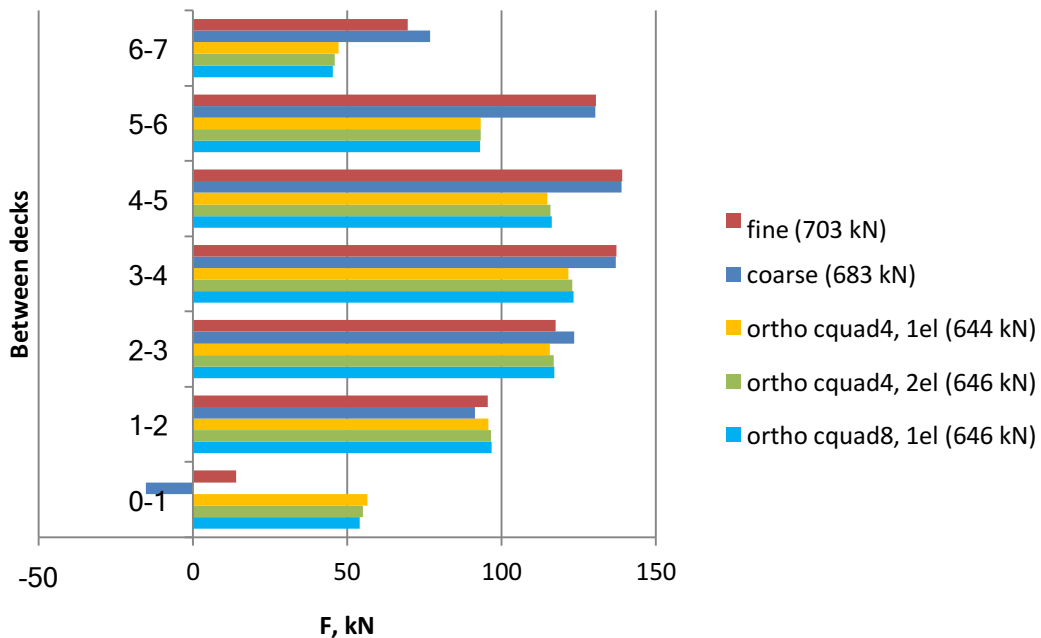


Figure 4.20 Vertical shear forces in side shell of box-like ship, region 1, M2 offset openings.

4.4.2 Performance of modeling techniques at high strain gradient areas

To evaluate accuracy of orthotropic model in case the loading on adjacent openings is significantly different (the stress and strain field cannot be considered periodic) the box-like ship model M2 with central openings was modified by replacing the longitudinal bulkhead at deck 3-4 with pillar line. The modified model is presented on Figure 4.21. As a result, the majority of vertical shear force flows through side shell between decks 3-4 instead of pillar line which has low shear stiffness compared to side shell as illustrated on Figure 4.21.

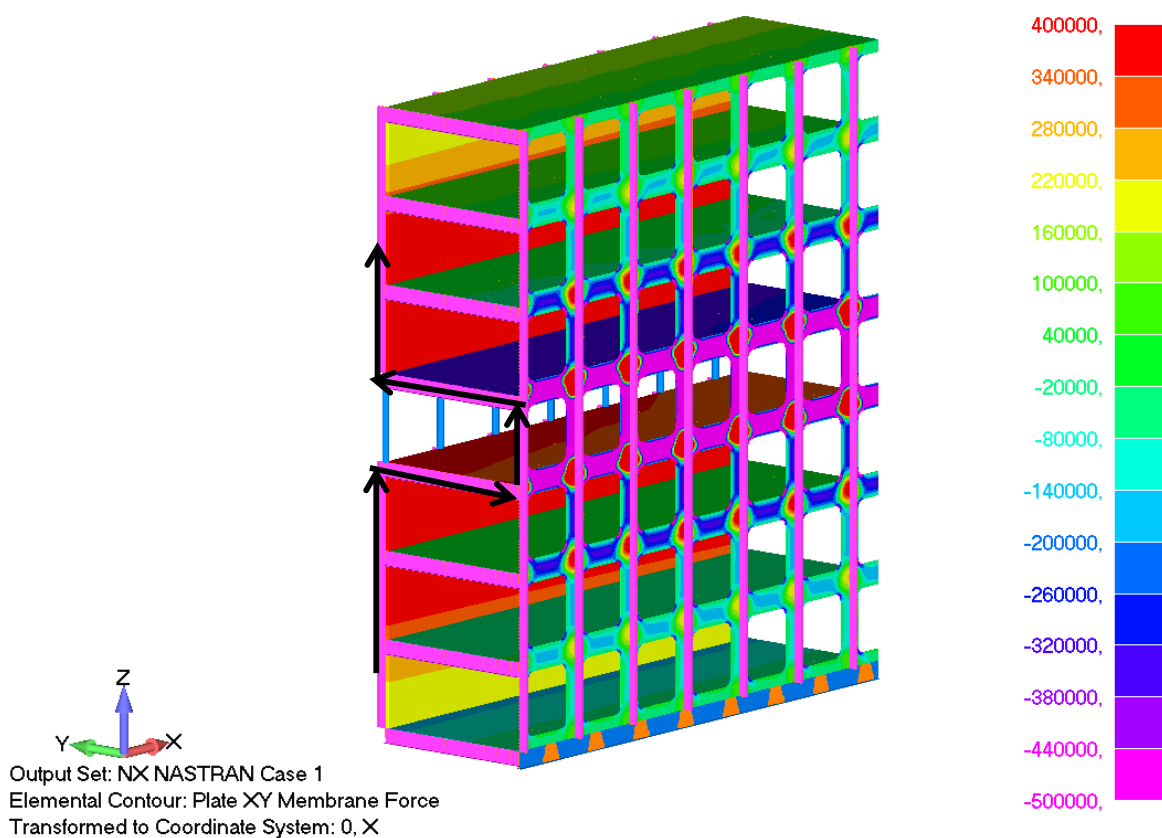


Figure 4.21 Explicit model of modified box-like ship model. Majority of shear flow, central openings.

The global deflection of fine, coarse and orthotropic model are 105,1 mm, 104,2 mm and 109,5 mm respectively, coarse mesh model is 0,9% less and orthotropic 4,2% more flexible. Comparison of vertical shear forces in region 1 is presented on figure 4.22. It is seen that in addition to errors at boundaries of the model, there is significant difference between reference and orthotropic model side shell shear forces at deck 3-4 and adjacent decks. In case of model with continuous longitudinal bulkhead the error in vertical shear force at these decks was only 10%. The significant

error is explained by large strain gradients arising due to violation of uniform loading assumption as discussed in chapter 2.4.2.

In contrast to orthotropic model, the coarse mesh model shows reliable vertical shear force around high strain gradient area as shown on Figure 4.22. The reliability of coarse mesh model is also seen from accurate longitudinal deck forces on Figure 4.23. In case of orthotropic model, the hull girder bending response at deck 3-4 is less accurately modelled. This shows that for orthotropic modelling not only periodicity of structure is required but close to uniform load is needed for reasonable accuracy. Later should be taken account, when orthotropic modelling is applied in areas where discontinuous longitudinal bulkheads are present and sliding between deck levels depends largely on side shell shear stiffness. In such cases coarse mesh modelling should be considered as the reliability of response is better.

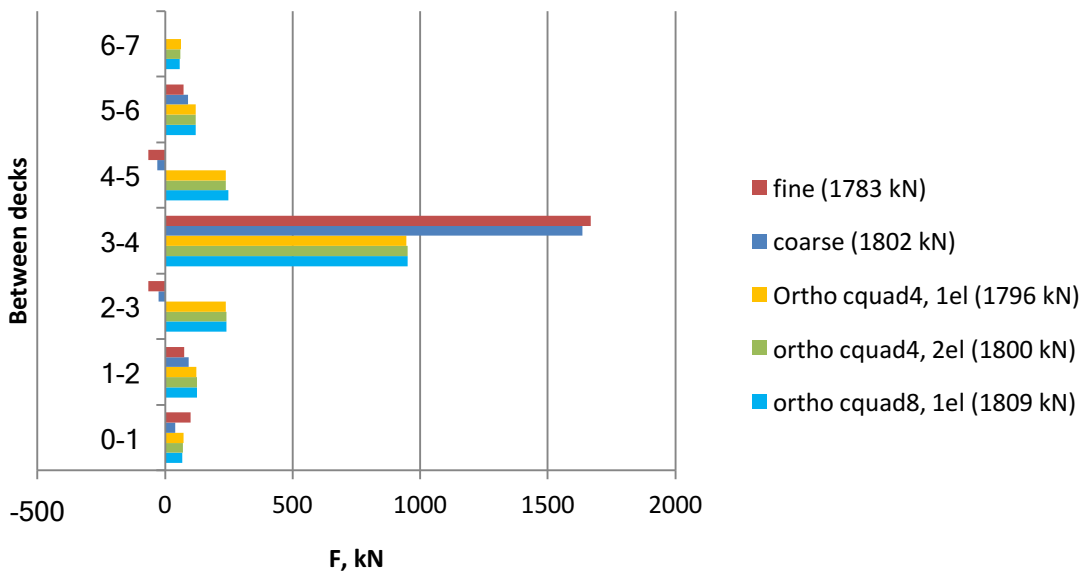


Figure 4.22 Vertical shear forces in side shell of modified box ship, region 1, central openings.

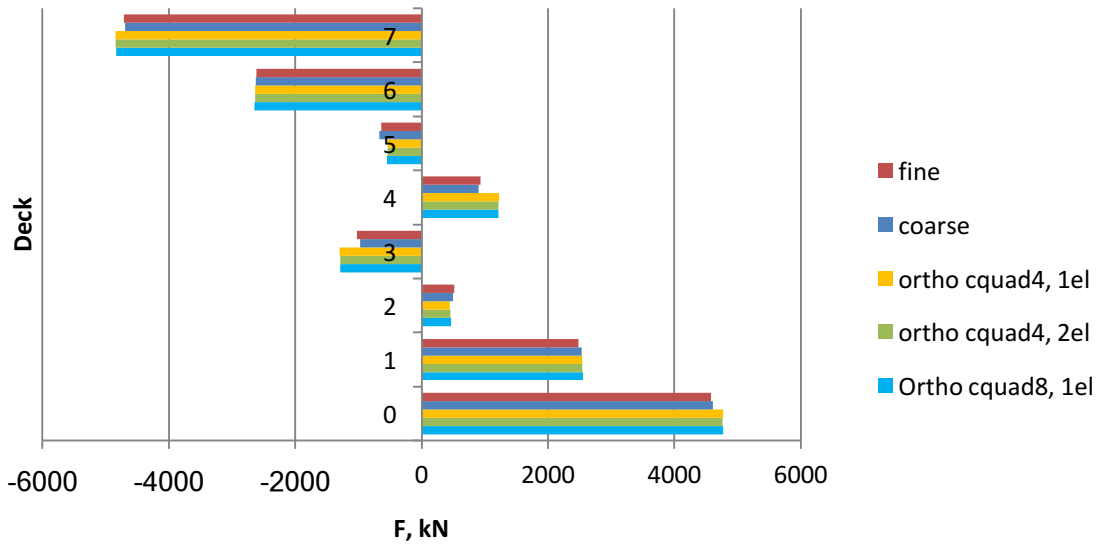


Figure 4.23 Longitudinal force in decks of modified box ship, region 2, central openings.

5. CONCLUSIONS

The aim of the thesis was to investigate applicability and develop a modeling approach for equivalent orthotropic and coarse mesh modeling of ship's central and stiffened offset side shell openings. The applicability was first assessed by tests on semi-global scale of side shell. Next, the approaches were evaluated in box-like ship to study the performance of modeling techniques in a periodic side shell, at its boundaries and at periodic side shell where large strain gradients are present.

For equivalent orthotropic modeling limitations of applicability were established. It was shown that in case of homogenizing offset openings according to classical theory the equivalent material behavior is orthotropic and coupling between shear and axial terms is zero. The necessity to include structural detail such as stiffeners for derivation of equivalent shear modulus was determined, which has not been covered in past studies [6], [18], [22], [25]. In addition, it was shown that in case of offset openings micropolar effect is present and the classical theory of elasticity is not valid as it assumes symmetric stress tensor and does not account for moments resulting from asymmetric stress distribution on RVE. For accurate local response a couple-stress theory [24] should be applied. This allows asymmetric stress tensor and moments per unit area. Despite compromised local response in side shell, the effect of micropolar behavior to global response was shown to be small.

While inaccuracy of orthotropic modeling at boundaries of periodic structure is well known, it was demonstrated that accuracy is also compromised at locations adjacent to discontinuous internal longitudinal bulkheads where large strain gradients occur. These limitations of boundary effect and strain gradients can be tackled by computational homogenization methods described by Geers in [19]. This approach is not however implemented into commercial FEA packages such as NX Nastran 11.

For coarse mesh modeling a mesh size sensitivity analysis for shear stiffness was performed for central and offset balcony openings inside a grid of similar openings. The contribution due to simplification of structure was taken account. Later has been covered only for corner radii and centrally placed openings in [25]. Coarse mesh modeling was shown to be sufficiently accurate for obtaining global and local response independent of large strain gradients. More significant errors in local response were detected at boundary areas due to coarse mesh's inability to accurately model localized deformations.

For reliable and efficient response estimation following notes about modeling techniques should be considered:

- Both, orthotropic and coarse mesh modelling result in sufficiently accurate global deflection and longitudinal bending response provided that equivalent properties are accurately derived and coarse mesh is verified by sensitivity analysis of shear stiffness.
- Accuracy of global response in orthotropic modeling is reduced when high strain gradients are present, which occurs when internal longitudinal bulkheads adjacent to side shell are discontinuous.
- Local response accuracy of orthotropic modeling depends on periodicity of structure and presence of large strain gradients. At boundaries of periodic grid and where high strain gradients are present, the local response accuracy is significantly compromised.
- The response of orthotropic model does not significantly vary if single or two 4-noded elements or single 8-noded element per opening is used.
- The coarse mesh model gives more reliable local side shell and global bending response at boundaries of periodic grid.
- Coarse mesh accuracy is not significantly compromised at locations of significantly non-uniform loading.

In future works, it is proposed that orthotropic and coarse mesh modeling as described in this thesis shall be tested in realistic ship models for evaluation of global response accuracy. Considering limitations of orthotropic modeling (boundary effect, large strain gradients, evolving opening geometry), it is suggested to investigate implementation of second order computational homogenization methods [20] to model periodic structures in scope of marine structures. These tackle the issues of boundary effect and large strain gradients as well as evolving microstructure eg. changing opening geometry.

5. KOKKUVÕTE

Töö eesmärk oli uurida ja arendada ortotroopse ning jämeda võrega modelleerimise rakendamist laeva tsentraalsete ja ekstsentriliste avadega küljekorpusele. Esimese sammuna hinnati meetodite täpsust perioodilises struktuuris rakendatuna perioodiliste avadega küljekorpusele. Lisaks uuriti modelleerimistehnikaid prismaatilise laeva mudelis hindamaks meetodite täpsust perioodilise struktuuri äärtes ja piirkondades kus esinevad suured moondegradiendid.

Ekvivalentse ortotroopse tehnika rakendamisel ekstsentrilistele ja tsentraalsetele avadele, kasutades homogeniseerimist klassikalise elastsusteooria järgi, on materjali omadused ortotroopsed ja normaal- ning nihkepinge komponendid teineteisest sõltumatud. Töös leiti, et ekvivalentsete materjaliomaduste tuletamisel tuleks arvesse võtta ka jäigastajate mõju paneeli lõikejäikusele. Viimast pole erialases kirjanduses [6], [18], [22], [25] varasemalt arvesse võetud. Lisaks näidati, et ekstsentriliste avade homogeniseerimisel ilmneb mikropolaarne efekt, mida klassikaline materjalikäsitlus ei kirjelda kuna eeldatakse sümmeetrilist pingetensorit ja ei arvesta asümmeetrilisest pingeaotusest tulenevaid momente ühikrakul. Täpsema lokaalse pingeseisundi kirjeldamiseks tuleks rakendada *couple-stress* teooriat. Viimane võimaldab asümmeetrilist pingetensorit ja elementaarpinna esinevaid momente. Hoolimata lokaalsest ebatäpsusest on mikropolaarse efekti mõju globaalses mastaabis väike.

Kirjandusest ja teooriast oli teada, et ortotroopse tehnika täpsus perioodilise struktuuri äärtes väheneb. Lisaks sellele näidati, et meetodi täpsus kahaneb ka piirkondades, kus ilmnevad suured moondegradiendid. Moondegradiendid on tihti tingitud küljekorpusega kohakuti olevast mittepidevast vaheseinast. Et vältida moondegradientidest ja ääre efektist tulenevaid ebatäpsusi võib rakendada *computational homogenization* meetodit, mida on kirjeldatud Geers'i publikatsioonis [19]. Viimast meetodit pole aga rakendatud kommertslikesse lõplike elementide analüüsi programmidesse nagu NX Nastran 11.

Jämeda võrega mudeli jaoks tehti lõikejäikuse tundlikkuse analüüs võre suurusest nii perioodilise tsentraalsele kui perioodilise ekstsentrilise ava korral. Lisaks võeti arvesse geomeetria lihtsustuse mõju lõikejäikusele. Struktuuri lihtsustuse mõju on varasemalt arvestatud vaid ava nurkade raadiuse ära jätmise suhtes tsentraalse ava korral [25]. Jämeda võrega mudel andis rahuldavaid tulemusi nii globaalses kui lokaalses mõttes sõltumata suurte moondegradientide ilmnemisest. Märkimisväärsed ebatäpsused esinesid vaid perioodilise struktuuri äärtes kuna jäme võre ei võimalda piisava täpsusega kirjeldada lokaliseerunud deformatsioone.

Usaldusväärse ja efektiivse mudeli koostamisel tuleks arvesse võtta järgnevaid tulemusi:

- Nii ortotroopne kui jämeda võrega mudel võimaldavad hinnata rahuldava täpsusega globaalset läbipainet ja paindepingete jaotust eeldusel, et ekvivalentsed materjalomadused on tuletatud õigetel eeldustel ja jämeda võre suurus on löikejäikuse tundlikuse analüüsiga kooskõlas.
- Ortotroopse mudeli globaalset täpsust vähendavad suured moondegradiendid, mis esinevad kui küljekorpusega kohakuti olevad pikkivaheseinad pole pidevad.
- Ortotroopse mudeli lokaalne täpsus sõltub struktuuri perioodilisusest ja suurte moondegradientide ilmnemisest. Perioodilise võre äärtes ja suure moodnegradiendiga piirkondades ei ole ortotroopne mudel lokaalsete sisejõudude ja deformatsiooni hindamiseks usaldusväärne.
- Ortotroopse mudeli täpsus ei sõltu oluliselt ekvivalentse elemendi sõlmpunktide arvust.
- Jämeda võrega mudel kirjeldab parema täpsusega lokaalseid sisejõudusid ja siirdeid ning annab täpsemaid tulemusi struktuuri äärtes.
- Jämeda võrega mudeli täpsus ei sõltu oluliselt suurtest moodnegradientidest.

Edaspidistes töodes soovitatakse rakendada siin pakutud tehnikaid realistlikus laeva globaalmodelis, et hinnata meetodite täpsust juhul, mil perioodilise struktuuri osakaal on piiratud ja koormamine kompleksne. Arvestades ortotroopse tehnikaga kaasnevaid piiranguid (ääre efekt, suured moonde gradiendid, muutuv avade geometria) soovitatakse uurida teist järku *computational homogenization*'i meetodite rakendatavust laeva perioodiliste struktuuride modelleerimisel. Viimane meetod võimaldab arvestada ääre efekti, suurte moondegradientide ja muutuva avade geometriaga.

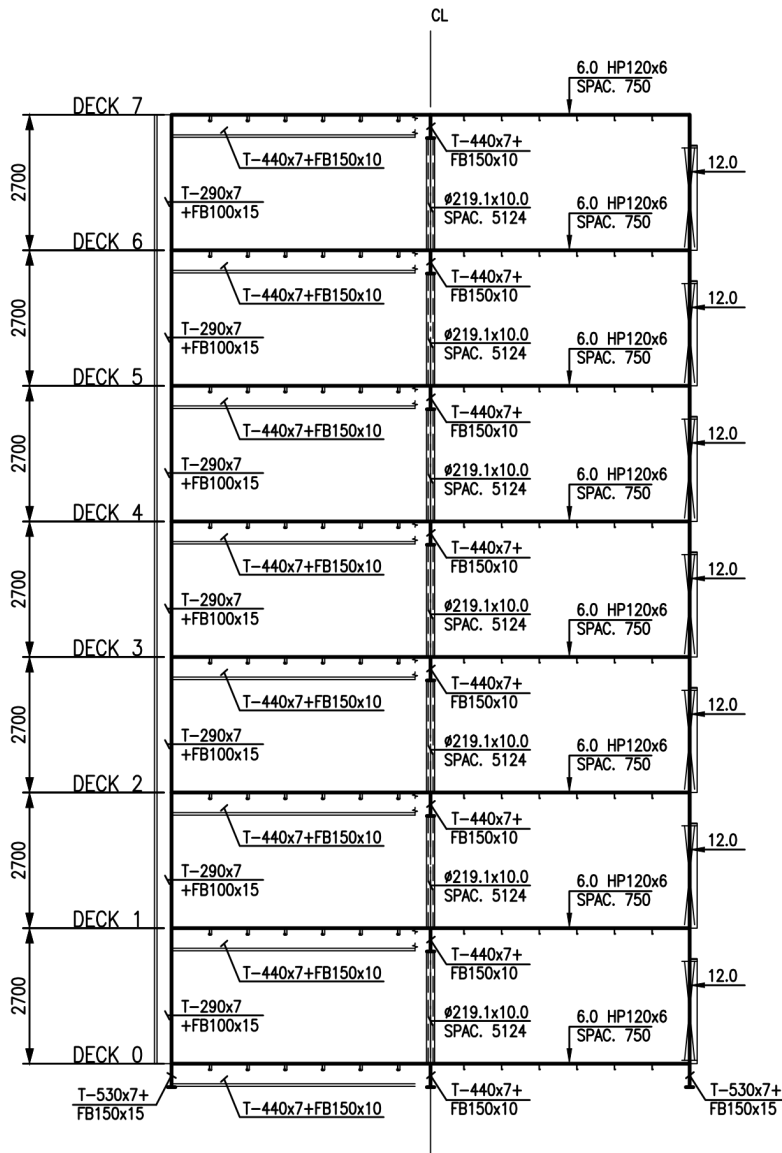
Bibliography

- [1] "Marine Traffic," 2017. [Online]. Available: <http://www.marinetraffic.com/en/ais/details/ships/shipid:288971/mmsi:249539000/imo:8512281/vessel:SOVEREIGN>. [Accessed 28 7 2017].
- [2] "Marine Traffic," [Online]. Available: http://www.marinetraffic.com/en/ais/details/ships/shipid:462106/mmsi:372067000/imo:8814263/vessel:CARIBBEAN_FANTASY. [Accessed 28 7 2017].
- [3] Cruise Industry News, [Online]. Available: <https://www.cruiseindustrynews.com/cruise-news/cruise-ship-orderbook.html>. [Accessed 28 7 2017].
- [4] C. G. Soares and Y. Garbatov, "MARSTRUCT," in *Progress in the Analysis and Design of Marine Structures: Proceedings of the 6th International Conference on Marine Structures*, Lisbon, 2017.
- [5] J. W. Fransman, "The influence of passenger ship superstructures on the response of the hull girder," in *RINA*, London, 1988.
- [6] V. Zanić and J. Andrić, "The global structural response model for multi-deck ships in concept design phase," *Ocean Engineering*, vol. 37, pp. 688-704, 2010.
- [7] E. Avi, I. Lillemäe, J. Romanoff and A. Niemelä, "Equivalent shell element for ship structural design," *Ships and Offshore Structures*, vol. 10, no. 3, pp. 239-255, 2013.
- [8] "DNV-GL Rules for Classification of Ships Pt. 5 Ch 4," 1 2017. [Online]. Available: <https://rules.dnvgl.com/docs/pdf/dnvgl/ru-ship/2017-01/DNVGL-RU-SHIP-Pt5Ch4.pdf>. [Accessed 20 2 2017].
- [9] A. Mobasher Amini, D. Dureisseix, P. Cartraud and N. Bua, "A domain decomposition method for problems with structural heterogenities on the interface: application to a passenger ship," *Computer Methods in Applied Mechanics and Engineering*, no. 198, pp. 3452-3463, 2009.

- [10] R. D. Cook, D. S. Malkus and M. E. Plesha, Concepts and Applications of the Finite Element Analysis, Wisconsin: John Wiley and Sons, 1989, pp. 257-260.
- [11] T. Zhodi, J. T. Oden and G. J. Rodin, "Hierarchical modelling of heterogeneous bodies," *Methods in Applied Mechanics and Engineering*, vol. 138, no. 1-4, pp. 273-298, 1996.
- [12] C. Farhat, M. Lesoinne, P. LeTallec, K. Pierson and D. Rixen, "FETI-DP: a dual-primal unified FETI method - part I: A faster alternative to the two-level FETI method," *International Journal for Numerical Methods in Engineering*, vol. 50, pp. 1523-1544, 2001.
- [13] C. Farhat, M. Lesoinne and K. Pierson, "A scalable dual-primal domain decomposition method," *Numerical Linear Algebra with Applications*, vol. 7, no. 7-8, pp. 687-714, 2000.
- [14] W. Fricke, B. Gerlach and M. Guiard, "Effect of Window Openings on the Stiffness of Walls and Bulkheads in ships," in *International Conference on thin-Walled Structures*, Busan, 2014.
- [15] K. Melk, Shear-Induced Secondary Bending Response at Balcony Opening of Passenger Ship. Master thesis, Espoo, 2011.
- [16] H. E. Jaeger and J. J. Woortman, "Some new Factors in the calculation of the Interaction between a Ship's Hull and a long Deckhouse," *Trans. of the Royal Inst. of naval Architects*, vol. 103, pp. 457-478, 1961.
- [17] C. T. Sun and R. S. Vaidya, "Prediction of composite properties from a representative volume element," *Composites Science and Technology*, vol. 56, pp. 171-179, 1996.
- [18] C. Amian, "Concept of modelling openings by means of shell elements with reduced in plane stiffness using orthotropic material properties," 2006.
- [19] M. G. D. Geers, V. Kouznetsova and W. Krekelmans, "Multi-scale computational homogenization: Trends and challenges," *Journal of Computational and Applied Mathematics*, vol. 234, pp. 2175-2182, 2010.
- [20] V. Kouznetsova, M. Geers and W. Berkelmans, "Multi-scale second-order computational homogenization of multi-phase materials: a nested finite element solution strategy," *Comput. Methods Appl. Mech. Engrg*, vol. 193, pp. 5525-5550, 2004.

- [21] R. H. Macneal, "A simple quadrilateral shell element," *Computers & Structures*, vol. 8, no. 2, pp. 175-178, 1978.
- [22] M. Heder and A. Ulfvarson, "Hull Beam Behaviour of Passenger Ships," *Marine Structures*, vol. 4, no. 1, pp. 17-34, 1991.
- [23] Z. P. Bažant, "Micropolar medium as a model for buckling of grid frameworks," in *Proc. , 12th Midwestern MEchanics Conference*, University of Notre Dame, 1971.
- [24] L. Shutian and S. Wenzheng, "Effective couple-stress continuum model of cellular solids and size effects analysis," *International Journal of Solids and Structures*, vol. 46, pp. 2787-2799, 2009.
- [25] B. G. Wolfgang Fricke, "Effect of large openings without and with windows on shear stiffness of side walls of passenger ships," *Ships and Offshore Structures*, vol. 10, no. 3, pp. 256-271, 2014.
- [26] E. Avi, Equivalent shell element for ship structural design. Master thesis, Espoo, 2012.
- [27] T. Holmberg, Rapid Finite Element Analysis of a Passenger Ship. Master Thesis, Espoo, 2001, p. 108.

APPENDIX 1. SCANTLINGS OF BOX-LIKE SHIP

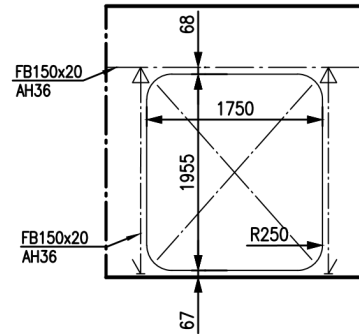


PRINCIPAL DIMENSIONS:

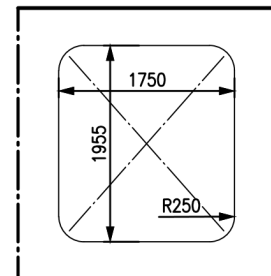
LENGTH 92.232 m
 BREADTH 10.16 m
 HEIGHT 19.43 m

NOTES:

ALL SIDE SHELL OPENINGS ARE OFFSET TYPE FOR MODEL WITH OFFSET OPENINGS;
 ALL SIDE SHELL OPENINGS ARE CENTRAL TYPE FOR MODEL WITH CENTRAL OPENINGS



OFFSET SIDE SHELL OPENING (2:1)



CENTRAL SIDE SHELL OPENING (2:1)

WEB FRAME (SPAC. 2562) DECK STIFFENER SPACING 750

Based on	Rev.	Copyright of Meyer Turku Oy. All rights reserved. No part thereof may be disclosed, copied, duplicated or in any other way made use of, except with the prior approval of Meyer Turku Oy. Also any unauthorized possession of this document is prohibited without the prior approval of Meyer Turku Oy.									
Part of	Rev.										
Replaces	Rev.										
Design	Martin Kaldoja	<h1>Meyer Turku</h1> <p>BOX LIKE SHIP "M1"</p>									
Compay											
Tel.	Date 10.07.2017										
Check.											
Apprv.											
Program	AutoCAD 2018 Student version	Paper size	A4 (210x294)	Drawing number		Rev		Page	1	Pages	(1)
Mass		Scale	1:150								

PRINCIPAL DIMENSIONS:

LENGTH 92.232 m
 BREADTH 5.08 m
 HEIGHT 19.43 m

NOTES:

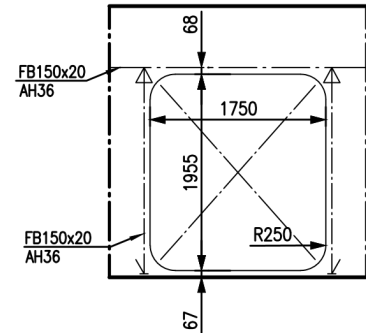
ALL SIDE SHELL OPENINGS ARE OFFSET TYPE FOR MODEL WITH OFFSET OPENINGS;
 ALL SIDE SHELL OPENINGS ARE CENTRAL TYPE FOR MODEL WITH CENTRAL OPENINGS



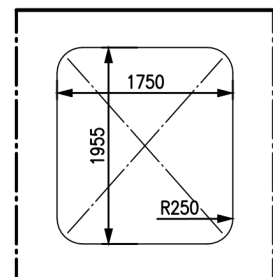
WEB FRAME (SPAC. 2562)

ORDINARY FRAME (SPAC. 854)

DECK STIFFENER SPACING 750



OFFSET SIDE SHELL OPENING (2:1)



CENTRAL SIDE SHELL OPENING (2:1)

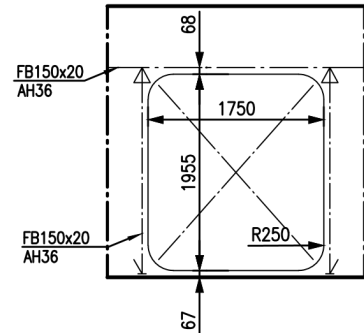
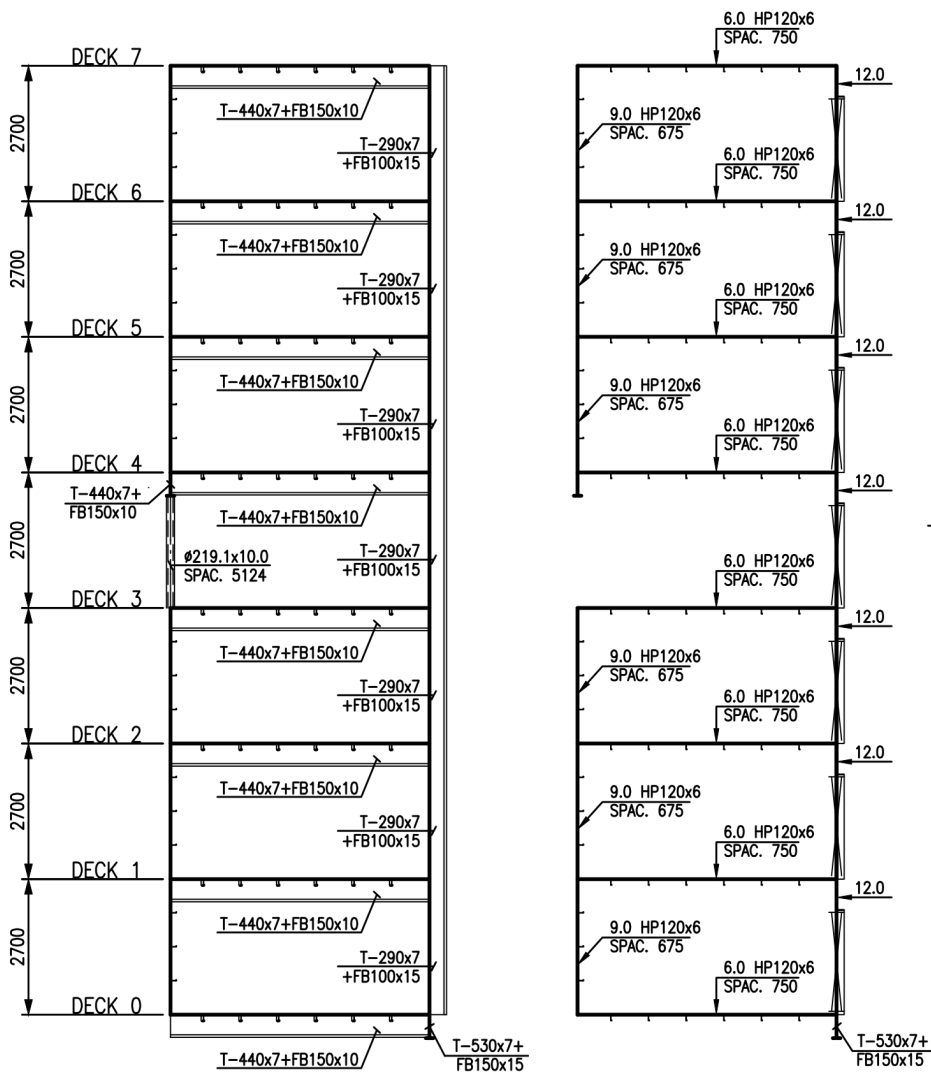
Based on	Rev.	Copyright of Meyer Turku Oy. All rights reserved. No part thereof may be disclosed, copied, duplicated or in any other way made use of, except with the prior approval of Meyer Turku Oy. Also any unauthorized possession of this document is prohibited without the prior approval of Meyer Turku Oy.					
Part of	Rev.						
Replaces	Rev.						
Design	Martin Kaldoja	<h1>Meyer Turku</h1> <p>BOX LIKE SHIP "M2"</p>					
Compay							
Tel.	Date 10.07.2017						
Check.							
Apprv.							
Program	AutoCAD 2018 Student version	Paper size	A4 (210x294)	Drawing number	Rev	Page	Pages
Mass		Scale	1:150			1	(1)

PRINCIPAL DIMENSIONS:

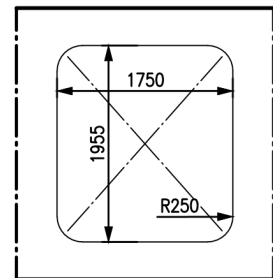
LENGTH 92.232 m
 BREADTH 5.08 m
 HEIGHT 19.43 m

NOTES:

ALL SIDE SHELL OPENINGS ARE OFFSET TYPE FOR MODEL WITH OFFSET OPENINGS;
 ALL SIDE SHELL OPENINGS ARE CENTRAL TYPE FOR MODEL WITH CENTRAL OPENINGS



OFFSET SIDE SHELL OPENING (2:1)



CENTRAL SIDE SHELL OPENING (2:1)

WEB FRAME (SPAC. 2562)

ORDINARY FRAME (SPAC. 854)

DECK STIFFENER SPACING 750

Based on	Rev.	Copyright of Meyer Turku Oy. All rights reserved. No part thereof may be disclosed, copied, duplicated or in any other way made use of, except with the prior approval of Meyer Turku Oy. Also any unauthorized possession of this document is prohibited without the prior approval of Meyer Turku Oy.
Part of	Rev.	
Replaces	Rev.	
Design	Martin Kaldoja	<h1>Meyer Turku</h1> <p>BOX LIKE SHIP "M2 MODIFIED"</p>
Compay		
Tel.	Date 10.07.2017	
Check.		
Apprv.		
Program	AutoCAD 2018 Student version	Drawing number
Mass	Paper size A4 (210x294)	Rev
	Scale 1:150	Page
		Pages

Meyer Turku

BOX LIKE SHIP "M2 MODIFIED"